REPORT DOCUMENTATION PAGE

Form Approved
OMB No. 0704-0188

1. AGENCY USE ONLY (Leave blank)	2. REPORT DATE	3. REPORT TYPE AND DATES COVERED
	8/17/94	Annual: 5/1/93-4/30/94

4. TITLE AND SUBTITLE
Theoretical and Experimental Studies of a Novel Accelerating Structure

5. FUNDING NUMBERS
ONR Contract
SFRC Number
N00014-91-J-1941

6. AUTHOR(S)
R. M. Gilgenbach and Y. Y. Lau

7. PERFORMING ORGANIZATION NAME(S) AND ADDRESS(ES)
Nuclear Engineering Department
University of Michigan
Ann Arbor, MI 48109-2104

8. PERFORMING ORGANIZATION REPORT NUMBER

9. SPONSORING/MONITORING AGENCY NAME(S) AND ADDRESS(ES)
Ballistic Missile Defense Organization
Innovative Science and Technology/
Office of Naval Research

10. SPONSORING/MONITORING AGENCY REPORT NUMBER

11. SUPPLEMENTARY NOTES

12a. DISTRIBUTION/AVAILABILITY STATEMENT
Approved for public release;
distribution is unlimited.

12b. DISTRIBUTION CODE

13. ABSTRACT *(Maximum 200 words)*

Research during the past year has concentrated on a novel, two-beam accelerator (twobetron) which was conceived. This idea was published in Physical Review Letters and a patent application was filed.
Accomplishments include the following:
1) Theoretical analysis of the new technique for phase-focusing this new accelerator,
2) Theory of e-beam modulation, BBU and other issues,
3) Initial generation and transport of an annular electron beam,
4) Design and fabrication of model/ prototype accelerator cavities, and
5) Initial cold tests of accelerator cavities.

14. SUBJECT TERMS	15. NUMBER OF PAGES
Electron beams, accelerators, beam-breakup-instability	29
	16. PRICE CODE

17. SECURITY CLASSIFICATION OF REPORT	18. SECURITY CLASSIFICATION OF THIS PAGE	19. SECURITY CLASSIFICATION OF ABSTRACT	20. LIMITATION OF ABSTRACT
UNCLASSIFIED	UNCLASSIFIED	UNCLASSIFIED	Unlimited

Table of Contents

1.0 Summary of Research Progress

Research during the past year has concentrated on a novel, two-beam accelerator (twobetron) which was conceived. This idea was published in Physical Review Letters and a patent application was filed. Accomplishments include the following:

1) Theoretical analysis of the new technique for phase-focusing this new accelerator,

2) Theory of e-beam modulation, BBU and other issues,

3) Initial generation and transport of an annular electron beam,

4) Design and fabrication of model/ prototype accelerator cavities, and

5) Initial cold tests of accelerator cavities.

2.0 Experimental Design

The experimental design for the Twobetron accelerator is shown in Figure 1. The driver beam is an annular electron beam, which initially is designed to carry about 500 A. This annular e-beam is to be modulated at 3.65 GHz by a two- cavity relativisitic klystron-amplifier (RKA). An annular RKA system was designed because the desired e-beam radius and frequency need to be cutoff to prevent RF leakage. After modulation, the annular e-beam passes through an array of TM_{02} microwave cavities with annular slots. The secondary electron beam will be initially generated by the center button of a velvet cathode. Although this e-beam will not be modulated when injected into the accelerating cavities, it will acquire its own modulation, in response to the modulated driver beam.

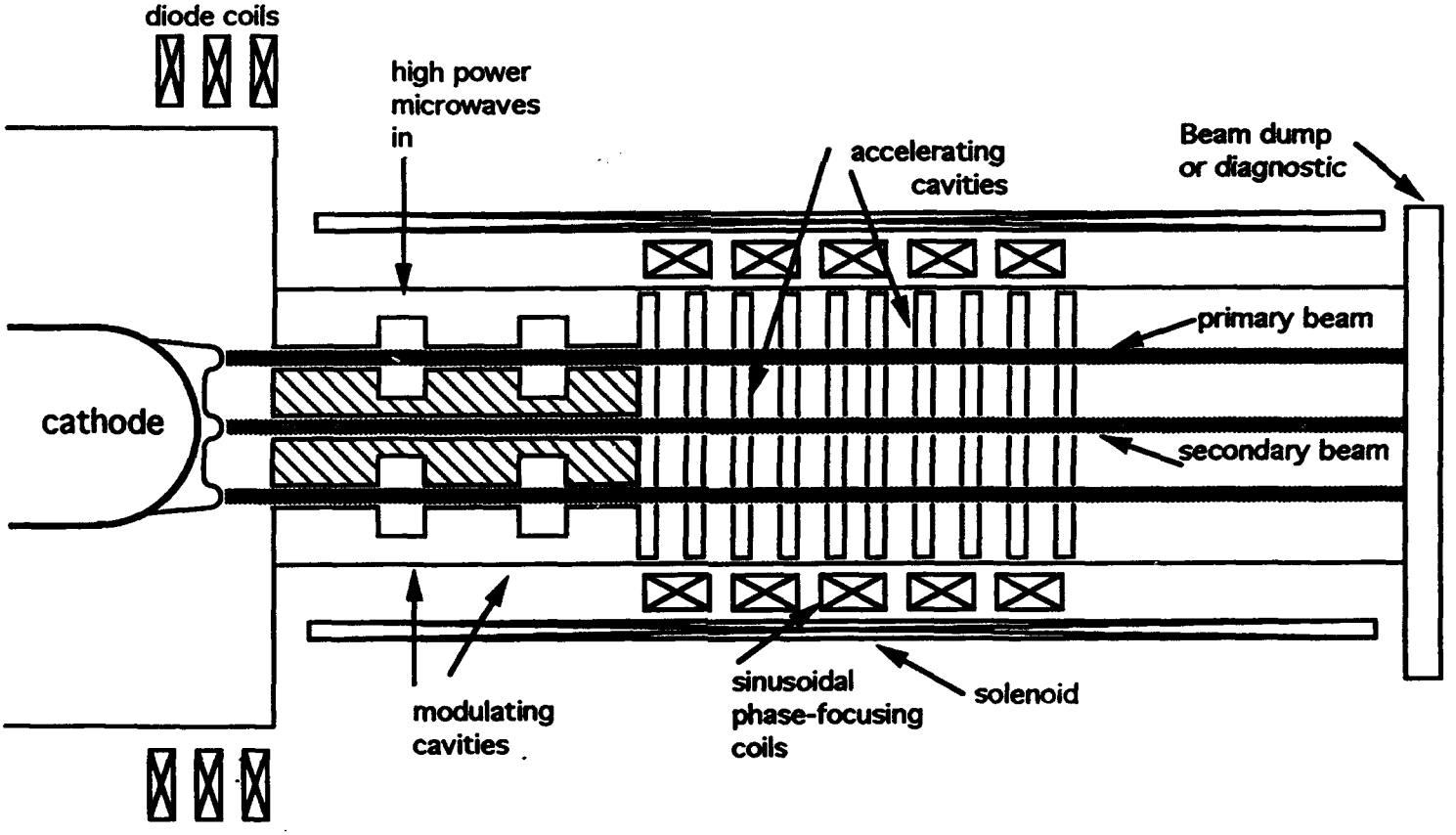

Figure 1. Experimental design

3.0 Experimental Results

3.1 Annular e-beam Generation and Transport

Electron beam experiments during the first year of the Two-Beam Accelerator project concentrated on the generation and transport of an annular electron beam. The annular e-beam cathode is depicted in Figure 2; a ring of velvet emitter was placed on a shaped aluminum cathode. The desired nonemitting region was coated with glyptal. Initial experimental results are shown in Figure 3, showing about 1.5 μs of the electron beam pulselength. On the waveform flattop sections (t=700ns), the diode current is about 5.4 kA; apertured current extracted through the anode is about 2.5 kA. Of the 2.5 kA extracted, about 1.3 kA was collected by a graphite plate located ~ 70 cm down the 15.2 cm-diameter transport tube. The magnetic field was about 3-4 kG in the transport tube. Since we only need about 500 A through the annular accelerator-cavity slots, these initial results are very promising.

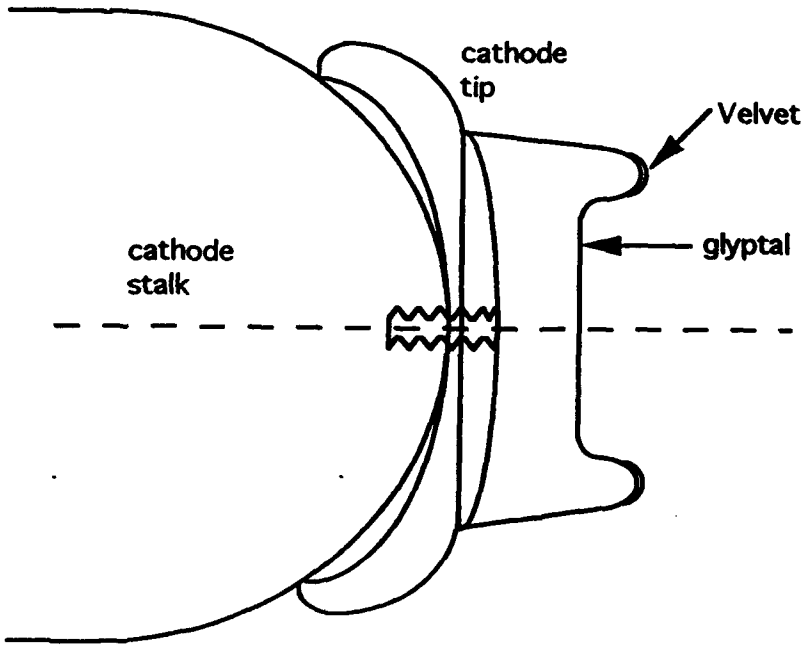

Figure 2. Annular e-beam cathode (initial trial).

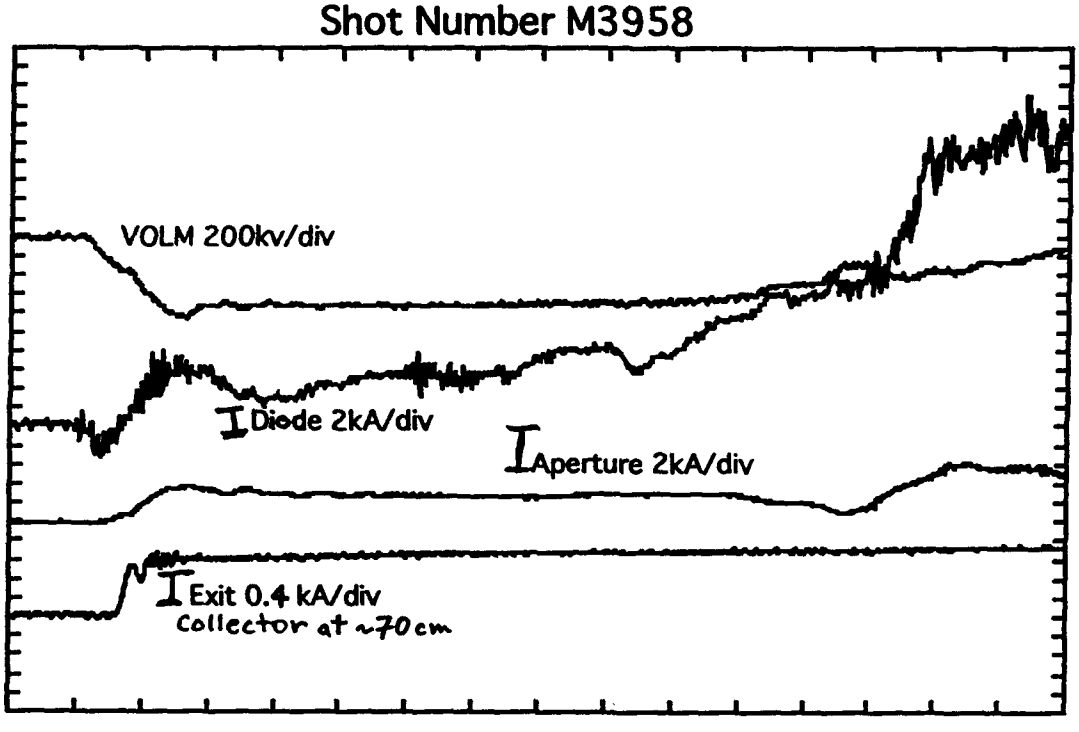

Figure 3. Experimental data from annular electron beam generation and transport.

3.2 Accelerator Cavity Design and Fabrication

A number of prototype accelerating cavities were designed and fabricated for cold testing. The first of these cavities, shown in Figure 4, employed three annular slots for the driver (primary) e-beam and a hole in the center for the secondary e-beam. Interpretation of initial cold-tests were difficult when the coupling was done through the center hole, so inductive coupling loops were utilized on a "blank" cavity with no slots; this produced much better results, which were obtained after the period of this report and will be described in a later report.

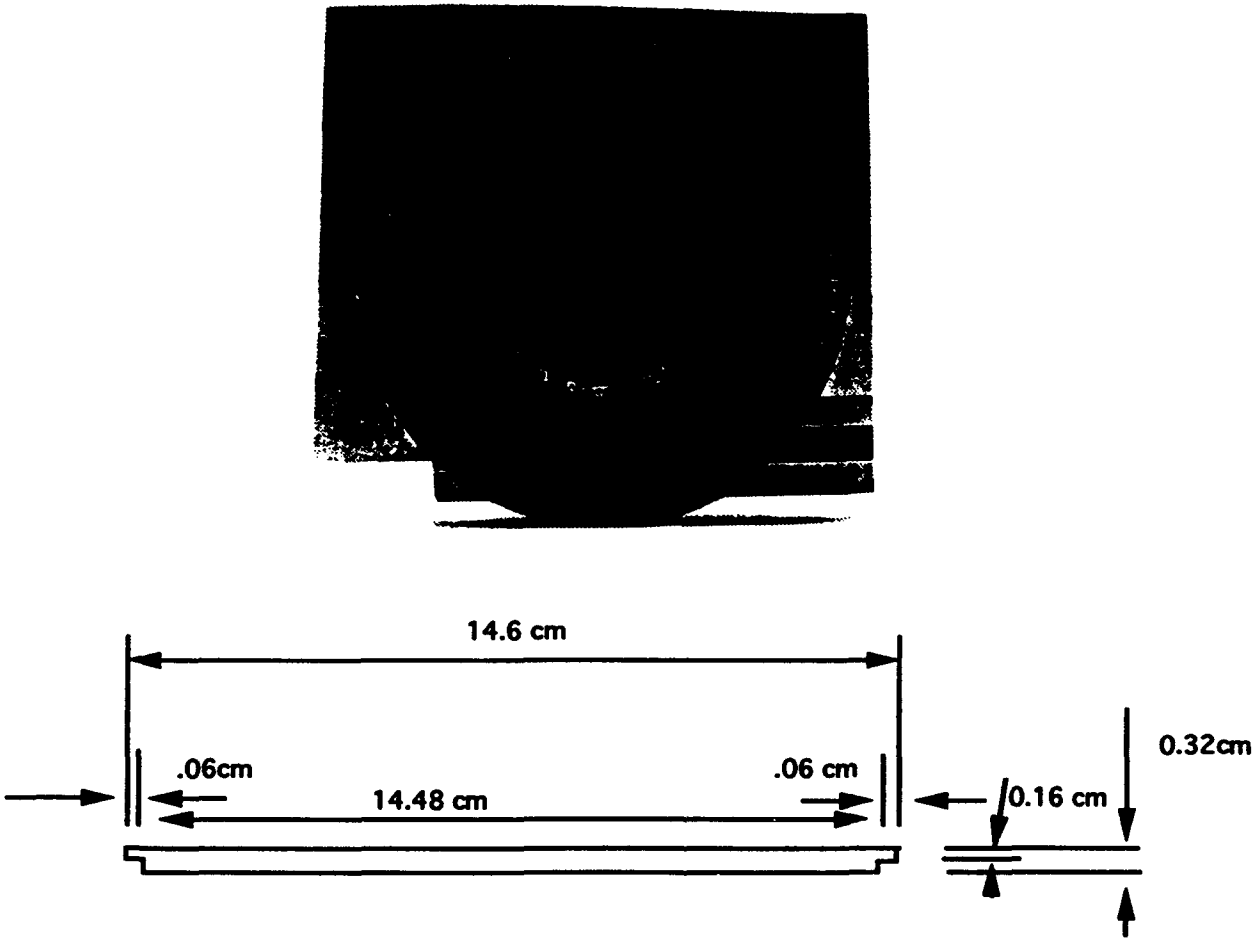

Figure 4. Initial accelerating cavity design.

4.0 Theoretical Results

4.1 Two Beam Accelerator

The concept of the novel two-beam accelerator has already been documented in our papers (attached) and will not be repeated here. We shall only address a few important issues that we have more recently examined. They concern the scaling laws, wakefield effects, effects of finite beam thickness, coupling among cavities, modification of rf characteristic by the intense driver beam, and the integrity of the primary beam modulation in the accelerating structure.

Scaling Laws

The average energy gain per cavity by the secondary beam in the twobetron is

$$\langle E_s \rangle = (16.3 \text{ keV}) \times Q \times (I_d/1\text{kA}) \times (\Delta/a)$$

where Q is the quality factor of the TM_{020} mode, I_d is the rf current on the driver beam, Δ is the amplitude of radius modulation, and a is the mean radius of the annular driver beam. The transformer ratio, R, which is the ratio of the energy gain in the secondary beam to the energy loss to the primary beam, is

$$R = 0.803\ (a/\Delta)$$

The maximum amount of secondary beam current, Is, that can be accelerated is limited to

$$I_s < I_d/2R$$

Given a driver beam current, we cannot make the acceleration gradient (i.e., $<E_S>$) excessively high by using a high Q cavity. Too high a value of Q would lead to formation of a virtual cathode in the primary beam. Another practical limit on $<E_S>$ is set by rf breakdown in the cavities.

In general, a transformer ratio R of the order of 10 seems achievable. A two-stage twobetron, in which the accelerated beam of the first stage is used as the driver beam in the second stage, will provide voltage multiplication by a factor of 100, while the output current is correspondingly much reduced .

Primary Beam Instabilties

The intense driver beam passing through a sequence of cavities are highly vulnerable to beam breakup instabilities (BBU). However, we have recently found that BBU in an annular beam may be far less serious than a pencil beam. Specifically, in the absence of other stabilizing mechanisms such as stagger tune and betatron frequency spread, the BBU exponentiates only 1.8 e-folds (in amplitude) for a 500 ns, 0.5 kA driver beam in a 90 cm accelerator structure embedded in a 10 kG solenoidal magnetic field.

We conjecture that the longitudinal (Robinson-like) instability probably is not important for the twobetron, at least in the proposed proof-of-principle experiment. Unlike a circular accelerator, the present scheme is single-pass. Its acceleration length is quite short, its length is only slightly over one wavelength in the radius modulation. Moreover, the drive frequency may be adjusted to be on the "right side" of the structure frequency to avoid the Robinson-like instability.

In a preliminary particle simulation, we find that the current modulation is preserved on the primary beam, after it is made to propagate through the accelerating structure, using the beam and structure parameters that are being planned for the proof-of-principle experiment.

RF Coupling Between Cavities

We have for simplicity assumed that the cavities are isolated from one another electromagnetically when the beam is absent. There are several ways to reduce the coupling among neighboring cavities. The inductive coupling at the annular slots, through which the driver beam passes, may be cancelled by the capacitive coupling at the center hole, and if necessary, by introducing additional holes near the rf electric field maximum (so as to increase the capacitive coupling) that is close to the outer wall of the cavity. Alternatively, conducting wires may be inserted radially across the annular gap to reduce the inductive coupling. Multiple pencil beams may also be used as the driver. These pencil beams pass through holes that are distributed annularly. In the event that the neighboring cavities are not completely isolated electromagnetically, a traveling wave formulation would be required; but the radius modulation that is proposed in this paper still provides an external control to ensure phase focusing.

The presence of intense space charge in the driver beam complicates matter substantially as it is known to modify the rf characteristics in an unpredictable manner. Such modifications include a detune of the structure frequency and modification of the gap transit-time factor, especially if a virtual cathode is at the verge of being formed. Other modes may be excited. Indeed, mode competition is a major area that requires considerable attention in the twobetron concept.

CONCLUDING REMARKS

In summary, the twobetron has the potential of converting many existing pulse power systems into compact rf accelerators that are suitable for industrial and medical applications. The driver beam is a modulated electron beam of annular shape and low energy. The secondary beam is an on-axis pencil beam. The secondary beam may reach an energy up to 10 MeV in one to two meters. Transformer ratio on the order of ten is considered feasible for each stage. Phase focusing and energy tunability of the accelerated beam may be provided by an external magnetic field, which controls the radius of the primary beam.

Excitation of the undesirable modes by the driver beam is perhaps the single most important issue in the twobetron concept.

5.0 Patent Application Filed

A patent application was filed on"Two-Beam Particle Acceleration Method and Apparatus" on February 18, 1994.

6.0 Honors and Awards

Y. Y. Lau received the Excellence in Research Award from the University of Michigan Nuclear Engineering Department in January 1994. Professor Lau was appointed Associate Editor of Physics of Plasmas, effective January 1994.

7.0 Publications Sponsored by This Project

1) "Proposal for a Novel Two-Beam Accelerator", Ya. S. Derbenev, Y. Y. Lau, and R. M. Gilgenbach, Physical Review Letters, 72 3025 (1994)

2) Beam breakup in an annular beam", Y.Y. Lau and J. Luginsland, Journal of Applied Physics 74 5877 (1993)

3) "Beam breakup growth and reduction experiments in long-pulse electron beam transport", P. R. Menge, R. M. Gilgenbach, Y. Y. Lau, and R. A. Bosch, Journal of Applied Physics, 75 1258 (1994)

Conference Papers

1) Beam breakup in an annular beam", Y.Y. Lau, J. Luginsland, and R. M. Gilgenbach, Presented at the 1993 Annual Meeting of the Division of Plasma Physics of the APS, St. Louis, MO

2) Y. Y. Lau, Ya. S. Derbenev, and R. M. Gilgenbach, "Novel, Compact Two-Beam Accelerator", Beams '94, San Diego, CA, June 20-24, 1994 (Published in Proceedings)

3) Advanced Accerator Workshop, Lake Geneva, WI, June 12-17, 1994

8.0 Personnel Involved in This Research

1) R. M. Gilgenbach, Professor

2) Y. Y. Lau, Professor

3) Ya. S. Derbenev, Visiting Research Scientist

4) John Luginsland, Graduate Student (Theory)

5) Jonathan Hochman, Graduate Student (Experiment)

6) Mark Walter, Graduate Student (Experiment)

Proposal for a Novel Two-Beam Accelerator

Ya. S. Derbenev, Y. Y. Lau, and R. M. Gilgenbach
Intense Energy Beam Interaction Laboratory, Department of Nuclear Engineering, University of Michigan, Ann Arbor, Michigan 48109-2104
(Received 1 November 1993; revised manuscript received 16 February 1994)

A new configuration is proposed wherein a low-current beam is accelerated to high energies (tens of amps, tens of MeV) by a driver beam of high current and low energy (a few kiloamps, < 1 MeV). The annular driver beam excites the TM_{020} cavity mode of an accelerating structure which transfers its rf power to the on-axis secondary beam. Systematic variation of the driver beam radius provides the secondary beam with phase focusing and adjustable acceleration gradient. A proof-of-principle experiment is suggested.

PACS numbers: 41.75.−i, 29.17.+w

Compact electron and ion accelerators in the 10 MeV range have a wide range of applications, such as treatment of bulk materials, activation analysis, and medical radiation sources. To achieve such an energy at moderate levels of current (tens of amps) requires considerable power, and a natural candidate for a driver is the pulse power system [1,2]. Intense annular electron beams (a few kiloamps, < 1 MeV) extracted from such a system have been modulated efficiently, and the current modulations exhibit a high degree of amplitude and phase stability [3]. These modulated beams have been used to generate ultrahigh power microwaves [4,5] and to accelerate electrons to high energies [6]. They will be used as the driver in the two-beam accelerator to be proposed in this paper.

Various two-beam accelerators have been studied in the past [6–10]. There are significant differences in the present configuration, shown schematically in Fig. 1. The driver beam is an annular beam of radius r_0, carrying an ac current I_d at frequency ω. It passes through an accelerator structure, consisting of N cylindrical pillbox cavities. Each cavity has a radius $b = 5.52c/\omega$ so that ω is also the resonant frequency of the TM_{020} mode of the pillbox cavity (Fig. 1). The secondary beam is an on-axis pencil beam, carrying an ac current I_s ($I_s \ll I_d$), also at frequency ω. Since the rf electric fields of the TM_{020} mode have opposite signs in the outer region and in the inner region, the mode retards the annular driver beam but accelerates the on-axis secondary beam. As we shall see, if the driver beam radius is modulated axially, phase focusing and tunability in the output energy of the secondary beam can be achieved. This is the crucial feature of the present device, not shared by the prior works [6–10].

Thus, without the use of rf plumbing, the present scheme provides the gradual conversion of the primary beam power to the secondary beam over many accelerating gaps. Since the current modulation on the primary beam has been shown to be insensitive to the variations in the diode voltage and diode current [3], the effectiveness in the acceleration of the secondary beam is likewise insensitive to such variations.

To calculate the excitation of the TM_{020} mode by the primary beam, and the resultant acceleration of the secondary beam by this mode, we assume that the intense space charge on the beam does not alter the rf characteristic of the cavities [4,11,12]. We also assume that the individual pillbox cavities are electromagnetically isolated from each other when the beams are absent [13,14]. Since the cavities are excited mainly by the rf current I_d carried by the primary beam, the TM_{020} mode so excited *always decelerates* the primary beam electrons on the average (by conservation of energy). This is true whether the beam radius r_0 is larger or smaller than a, where $a = 2.405c/\omega$ is the radius of the rf electric field null of the TM_{020} mode [Fig. 2(a)]. The value of the rf electric field at r_0 then gives the deceleration gradient. In terms of the relativistic mass factor (γ_d), the energy loss by this driver beam as it traverses the nth cavity is given by

$$\frac{d\gamma_d}{dn} = -\Lambda\delta^2 \tag{1}$$

in a continuum description. In Eq. (1),

$$\Lambda = 0.066(\omega L/c)Q(I_d/1\ \mathrm{kA}) \tag{2}$$

is the dimensionless parameter that measures the strength of the cavity excitation by the primary beam,

$$\delta = J_0(\omega r_0/c) \approx -1.249(r_0 - a)/a\,, \tag{3}$$

Q is the quality factor of the TM_{020} mode, L is the cavity length, and J_0 is the Bessel function of the first kind of

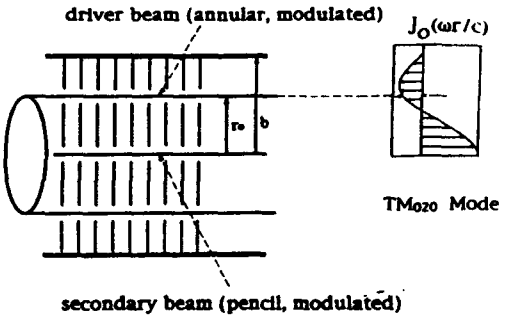

FIG. 1. Schematic drawing of the two-beam accelerator. Also shown is the rf force profile, $J_0(\omega r/c)$, associated with the axial electric field of the TM_{020} cavity mode.

0031-9007/94/72(19)/3025(4)$06.00

A-1

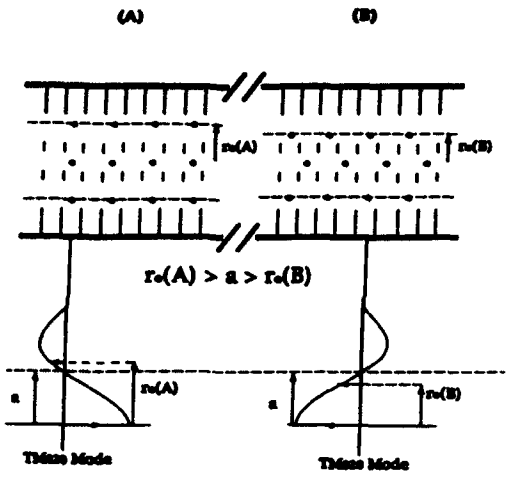

FIG. 2. (a) Position of the primary beam radius r_0 ($r_0 > a$) for secondary beam acceleration when both beams enter the cavity at the same phase. (b) Position of the primary beam radius r_0 ($r_0 < a$) for secondary beam acceleration when both beams enter the cavity at 180° phase apart.

order zero. In writing the last expression of Eq. (3), we have made the assumption that the annular beam is located in the vicinity of the rf electric field null ($r_0 \approx a$).

If the secondary beam enters the cavity at the same phase as the primary beam, the former will be accelerated if $r_0 > a$, for in this case the rf fields experienced by both beams have opposite polarity [Fig. 2(a)]. Since the rf electric field has a radial dependence of $J_0(\omega r/c)$, it is obvious that $1/|\delta|$ is the "transformer ratio," which is the ratio of the energy gain by the secondary beam to the energy loss by the primary beam, *if both beams enter the cavity at the same phase.* This dependence on the phase is reflected in the following equation which describes the change in the relativistic mass factor (γ_s) of the secondary beam as it traverses the nth cavity:

$$\frac{d\gamma_s}{dn} = -\Lambda\delta\cos(\theta_s - \theta_d), \tag{4}$$

where θ_s is the phase of the secondary beam bunch and θ_d is the phase of the primary beam bunch when they enter the nth cavity. Equation (4) is readily obtained from Eq. (1) by noting the transformer ratio $1/\delta$ and the phase difference mentioned above. Equations (3) and (4) indeed show that γ_s increases if $r_0 > a$ and if $\theta_d = \theta_s$.

The secondary beam cannot be accelerated indefinitely because of the increase in the phase slippage between θ_d and θ_s downstream. This phase slippage occurs as the primary beam is decelerated and the secondary beam is accelerated. Its rate of increase is governed by

$$\frac{d(\theta_s - \theta_d)}{dn} = \frac{\omega L}{c}\left(\frac{1}{\beta_s} - \frac{1}{\beta_d}\right) = \frac{\omega L}{c}[(1 - 1/\gamma_s^2)^{-1/2} - (1 - 1/\gamma_d^2)^{-1/2}]. \tag{5}$$

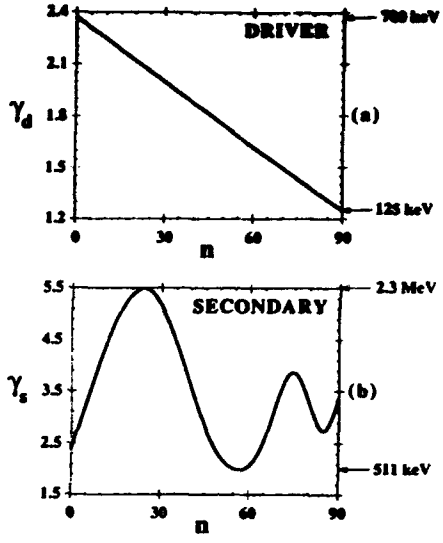

FIG. 3. Evolution of the relativistic mass factors when the driver beam radius r_0 is a constant: (a) the driver beam, (b) the secondary beam. Phase slippage prohibits continual acceleration of the secondary beam.

The effect on the secondary beam by this phase slippage is illustrated in Fig. 3, which is obtained by numerically solving the system of three equations [(1), (4), (5)] in three unknowns: γ_d, γ_s, and $\theta_s - \theta_d$. The initial conditions for these three unknowns are taken to be $\theta_s - \theta_d = 0$ and $\gamma_d = \gamma_s = 2.37$, corresponding to an initial energy of 700 keV for both beams. The other parameters are $\omega/2\pi = 3.65$ GHz, $b = 7.221$ cm, $L = 1$ cm, $a = 3.146$ cm, $r_0 = 3.322$ cm, $Q = 100$, and $I_d = 0.5$ kA. Since we have taken $L = 1$ cm, the cavity number n is also the axial distance (z) in cm.

Figure 3(a) shows that γ_d decreases from the initial value of 2.37 to 1.24 at $n = 90$; i.e., the primary beam's energy steadily decreases from 700 to 125 keV after propagating 90 cm. The secondary beam's energy [Fig. 3(b)] increases initially, reaching a maximum value of 2.3 MeV after 24 cm, and then decreases due to the phase slippage until $n = 56$, and oscillates further downstream as the phase slippage continues.

The phase slippage may be corrected by adjusting the primary beam's radius r_0. Consider, for example, the worst case of phase slippage where the primary beam and the secondary beam arrive at a cavity 180° out of phase, as shown in Fig. 2(b). If the primary beam's radius r_0 is *less* than a, it generates an rf electric field which would retard *both* beams during the time when the *primary* beam occupies the cavity. However, when the charge bunch of the primary beam resides in the cavity, there are few particles in the secondary beam residing in the same cavity because both beams arrive at the cavity 180° out of phase. By the time the charge bunch of the primary beam is about to leave the cavity, the rf electric field is about to change sign, at which time the charge bunch of the secondary beam is about to enter the cavity, whose rf electric field then begins to accelerate the entering bunch

A-2

on the secondary beam. Thus, the phase slippage problem can be corrected by a simple cure: At the locations where the bunches of both beams enter the cavity with the same phase, place r_0 outside a. When the bunches of both beams arrive at the cavity 180° out of phase, place r_0 inside a.

Mathematically, it is easy to see from Eqs. (3) and (4) that γ_s is a monotonically increasing function of n if r_0 is tapered in such a way that $(r_0-a)\cos(\theta_s-\theta_d)\geq 0$.

The above idea of phase slippage correction has been tested for the example shown in Figs. 3(a) and 3(b). From that figure, the phase slippage occurs with a period of the order of 75 cm. Thus, we correct the primary beam radius r_0 according to

$$r_0(\text{cm}) = 3.146 + (3.322 - 3.146)\cos(2\pi n/75). \quad (6)$$

Including only this modification, and keeping all other parameters the same, we obtain Fig. 4. In Fig. 4, we see that the primary beam's energy monotonically decreases from 700 to 400 keV over 90 cm, whereas the secondary beam's energy increases monotonically from 700 keV to a maximum of 4.2 MeV over the same distance, in sharp contrast to Fig. 3(b). The loss of 300 keV in the primary beam and the gain of 3.5 MeV in the secondary beam implies an effective transformer ratio of about (3.5 MeV)/(300 keV)=11.7.

In Fig. 4, the zero slopes in γ_s and in γ_d occur at the axial positions (n) at which the driver beam radius r_0 coincides with the field-null position a. The slight dip in γ_s at $n=90$ only means that the primary beam's radius r_0 needs further adjustment there. If we write $r_0 = a + \Delta\cos(\psi)$, where Δ is the amplitude and ψ is the phase of the modulation in r_0, the general phase focusing condition reads $d\psi/dn = d(\theta_s-\theta_d)/dn$. This condition is applicable when the two beams have different velocities. In fact, one might argue that this technique of radius modulation provides both beams with self-focusing in phase, similar to the self-focusing in synchrotrons [15].

The modulation in the annular beam radius may be readily achieved by a proper adjustment of the external solenoidal magnetic field which is often used for beam focusing and beam transport [3–6,14]. Since the rate of change of energy depends on the annular beam radius r_0 [cf. Eqs. (1) and (3)], the output energy of the accelerated beam may also be controlled by the same external magnetic field coils.

The above ideas may be tested in a proof-of-principle experiment with parameters similar to those used to produce Fig. 4. The primary beam may be obtained, for example, from the Michigan Electron Long-Beam Accelerator (MELBA) [16], which operates with diode parameters of 700 keV, current up to 10 kA, and flattop pulse length up to 1 μs. This primary beam may be modulated using the proven techniques by Friedman *et al.* [3,4,6]. Note that the average acceleration gradient of 40 kV/cm and the peak acceleration gradient of about 80 kV/cm implied by Fig. 4 are well within the rf breakdown limit. If we assume an acceleration efficiency of 25%, a secondary beam of more than 10 A of current may be accelerated to 4 MeV in less than a meter in this proof-of-principle experiment.

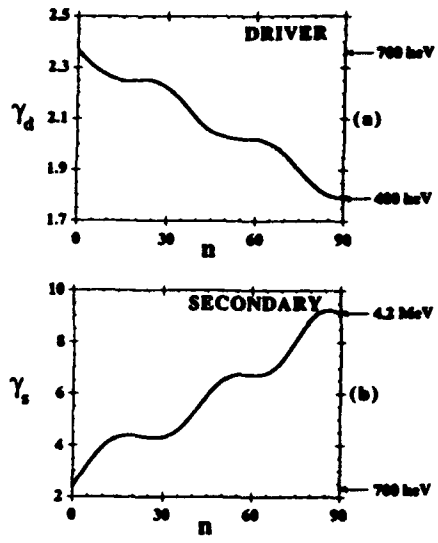

FIG. 4. Evolution of the relativistic mass factors when the driver beam radius r_0 is modulated to compensate phase slippage: (a) the driver beam, (b) the secondary beam.

There are many issues which may affect the eventual usefulness of the two-beam accelerator concept outlined above. Chief among them is the modification of the rf characteristic that always accompanies an intense driver beam, which includes a detuning of the structure frequency and a modification of the gap transit-time factor [4,11,12,17]. Also of concern is the beam breakup instability (BBU) on the driver beam [10,13,14,17]. However, we have recently found that BBU in an annular beam may be far less serious than a pencil beam [18], and BBU can be controlled by many well-known techniques [19]. The degree of coupling among neighboring cavities, especially in the presence of an intense beam, remains to be studied [20]. Although the driver beam's radius is a crucial factor, the effects of the beam's finite thickness are far less important, according to our preliminary studies. We have also examined the effects of the transverse wake [21] and of the longitudinal instabilities [22] and found that they are not serious, at least for the parameters used in the above numerical example, assuming a solenoidal field of 10 kG in the accelerating structure.

In summary, we propose a novel scheme which has the potential of converting many existing pulse power systems into compact rf accelerators that are suitable for industrial and medical applications. The driver beam is a modulated intense relativistic electron beam of annular shape and low energy (<1 MeV). The secondary beam is an on-axis pencil beam. The secondary beam may reach an energy up to 10 MeV in 1 to 2 m. Phase focusing and energy tunability of the accelerated beam may be provided by an external magnetic field, which controls the radius of the primary beam. While we have in this paper con-

A-3

centrated only on electron acceleration in the 10 MeV range, it is intriguing to speculate on the potential of using this technique (a) to accelerate ions to tens of MeV, and (b) to accelerate electrons to ultrahigh energy using superconducting cavities [cf. Eq. (2)] and higher energy driver beams.

We thank John W. Luginsland for assistance in the preparation of this manuscript. This work was supported by SDIO-BMD/IST/ONR.

[1] J. C. Martin (unpublished); see also the survey by J. A. Nation, Part. Accel. **10**, 1 (1979).

[2] S. Humphries, *Charged Particle Beams* (Wiley, New York, 1990); R. C. Davidson, *Physics of Nonneutral Plasmas* (Addison-Wesley, Redwood City, CA, 1990); R. B. Miller, *Intense Charged Particle Beams* (Plenum, New York, 1982).

[3] M. Friedman and V. Serlin, Phys. Rev. Lett. **55**, 2860 (1985); M. Friedman *et al.*, J. Appl. Phys. **64**, 3353 (1988); J. Krall and Y. Y. Lau, Appl. Phys. Lett. **52**, 431 (1988).

[4] M. Friedman *et al.*, Rev. Sci. Instrum. **61**, 171 (1990); Y. Y. Lau *et al.*, IEEE Trans. Plasma Sci. **18**, 553 (1990).

[5] See, e.g., Proc. SPIE Int. Soc. Opt. Eng. **1407** (1991); **1629** (1992); **1872** (1993) (edited by H. E. Brandt).

[6] M. Friedman *et al.*, Phys. Rev. Lett. **63**, 2468 (1989).

[7] M. A. Allen *et al.*, Phys. Rev. Lett. **63**, 2472 (1989); A. M. Sessler and S. S. Yu, *ibid.* **58**, 2439 (1987).

[8] G. Voss and T. Weiland, DESY Report No. M82-10, 1982 (unpublished); DESY Report No. M82-079, 1982 (unpublished).

[9] W. Gai *et al.*, Phys. Rev. Lett. **61**, 2765 (1988); H. Figueroa *et al.*, *ibid.* **60**, 2144 (1988); J. B. Rosenzweig *et al.*, Phys. Fluids B **2**, 1376 (1990).

[10] A. M. Sessler *et al.*, Part. Accel. **31**, 1277 (1990); Nucl. Instrum. Methods Phys. Res., Sect. A **306**, 592 (1991); D. B. Hopkins *et al.*, Nucl. Instrum. Methods Phys. Res. **228**, 15 (1984); D. H. Whittum *et al.*, Phys. Rev. A **43**, 294 (1991); also in "Advanced Accelerator Concepts," edited by J. Wurtele, AIP Conf. Proc. No. 279 (AIP, New York, to be published).

[11] P. B. Wilson, in *Physics of High Energy Particle Accelerators*, edited by R. A. Carrigan *et al.*, AIP Conf. Proc. No. 87 (AIP, New York, 1982), p. 452.

[12] D. G. Colombant and Y. Y. Lau, Phys. Rev. Lett. **64**, 2320 (1990).

[13] This is similar to the cumulative beam breakup instability, suggested by W. K. H. Panofsky and M. Bander, Rev. Sci. Instrum. **39**, 206 (1968).

[14] See, e.g., P. R. Menge, R. M. Gilgenbach, and Y. Y. Lau, Phys. Rev. Lett. **69**, 2372 (1992); Y. Y. Lau, *ibid.* **63**, 1141 (1989), and references therein.

[15] See, e.g., E. D. Courant, in *Physics of High Energy Particle Accelerators* (Ref. [11]), p. 2.

[16] R. M. Gilgenbach *et al.*, in *Digest of Fifth IEEE Pulse Power Conference* (IEEE, New York, 1985), p. 126.

[17] P. Menge, Ph.D thesis, University of Michigan, Ann Arbor, 1993.

[18] Y. Y. Lau and J. W. Luginsland, J. Appl. Phys. **74**, 5877 (1993). In the line above Eq. (7) of this paper, the factor [I/(1 kA)] should read [I/(17 kA)].

[19] In the absence of other stabilizing mechanisms such as stagger tune and betatron frequency spread, we estimate that a solenoidal magnetic field of 10 kG and a dipole mode Q of 100 would limit the *worst* BBU growth to $1.8e$-fold (in amplitude) for a 500 ns, 0.5 kA beam in a 90 cm accelerator structure, as in the numerical example.

[20] There are several ways to reduce the coupling among neighboring cavities. The inductive coupling at the annular hole, through which the driver beam passes, may be canceled by the capacitive coupling at the center hole, and if necessary, by introducing additional holes near the rf electric field maximum (so as to increase the capacitive coupling) that is close to the outer wall of the cavity (Fig. 1). Alternatively, conducting wires may be inserted radially across the annular gap to reduce the inductive coupling. Multiple pencil beams may also be used as the driver. These pencil beams pass through holes that are distributed annularly. In the event that the neighboring cavities are not completely isolated electromagnetically, a traveling wave formulation would be required; but the radius modulation that is proposed in this paper still provides an external control to ensure phase focusing.

[21] We estimate that a nominal value of solenoidal field $B_0 = 10$ kG would render the effects of the transverse wake field on the driver beam unimportant. Specifically, under the condition $\Omega \gg \omega/\gamma_d(1+\beta_d)$, where Ω is the nonrelativistic cyclotron frequency associated with B_0 and the other symbols are the same as in Eq. (5), the electron motion is adiabatic along the composite (dc+rf) magnetic field line. The maximum angular displacement, from the mean, is estimated to be $l_\theta = 0.52(c/\omega)(E_a/cB_0)\beta_d/(1-\beta_d)$ where E_a is the maximum accelerating electric field experienced by the secondary beam. The maximum radial displacement is $l_r = l_\theta \lambda_L/\lambda_m$, where $\lambda_L = 2\pi\beta_d\gamma_d c/\Omega$ and λ_m is the axial wavelength associated with the modulation in the driver beam radius. For the parameters used in the numerical example, $l_\theta \leq 0.2$ cm, and $l_r \leq 0.0058$ cm. The spread in momentum, dp, in the driver beam may introduce a variation in its annular beam radius, dr_0. It is estimated that $dr_0 \leq [2(\lambda_L^2/\lambda_m^2)\Delta + 0.083\lambda_L E_a/cB_0]dp/p$, where Δ is the amplitude of the modulation in the driver beam radius. Using the parameters in the numerical example, we find $dr_0 < 0.0061$ cm if $dp/p < 1$. Thus, the effectiveness of radius modulation is not affected by momentum spread.

[22] We conjecture that the longitudinal (Robinson-like) instability probably is not important for the present scheme, at least in the proposed proof-of-principle experiment. Unlike a circular accelerator, the present scheme is single pass. Its acceleration length is quite short; its length is only slightly over one wavelength in the radius modulation. Moreover, the drive frequency may be adjusted to be on the "right side" of the structure frequency to avoid the Robinson-like instability.

A-4

Beam breakup growth and reduction experiments in long-pulse electron beam transport

P. R. Menge,[a] R. M. Gilgenbach, Y. Y. Lau, and R. A. Bosch[b]
Nuclear Engineering Department, Intense Energy Beam Interaction Laboratory, University of Michigan, Ann Arbor, Michigan 48109-2104

(Received 19 August 1993; accepted for publication 26 October 1993)

The results of an experimental program whose sole objective is to investigate the cumulative beam breakup instability (BBU) in electron beam accelerators are presented. The BBU growth rate scalings are examined with regard to beam current, focusing field, cavity Q, and propagation distance. A microwave cavity array was designed and fabricated to excite and measure the cumulative BBU resulting from beam interactions with the deflecting TM_{110} cavity mode. One phase of this experiment used high $Q(\approx 1000)$ cavities with relatively large frequency spread $(\Delta f/f_0 \approx 0.1\%)$. The observed TM_{110} mode microwave growth between an upstream (second) and a downstream (tenth) cavity indicated BBU growth of 26 dB for an electron beam of kinetic energy of 750 keV, 45 A, and focused by a 1.1 kG solenoidal field. At beam currents of less than 100 A the experiments agreed well with a two-dimensional continuum theory; the agreement was worse at higher beam currents (>100 A) due to beam loading. The second-phase experiments used lower $Q(\approx 200)$ cavities with relatively low frequency spread $(\Delta f/f_0 \approx 0.03\%)$. Theory and experiment agreed well for beam currents up to 220 A. Distance scaling experiments were also performed by doubling the propagation length. Instability growth reduction experiments using the technique of external cavity coupling resulted in a factor of four decrease in energy in BBU growth when seven internal beam cavities were coupled by microwave cable to seven identical external dummy cavities. A theory invoking power sharing between the internal beam cavities and the external dummy cavities was used to explain the experimental reduction with excellent agreement using an equivalent circuit model.

I. INTRODUCTION

The beam breakup (BBU) instability is one of the most serious of the electron beam instabilities that arise in linear accelerators.[1] This instability results from the coupling of transverse beam oscillations and nonaxially symmetric electromagnetic modes of the accelerating structure. The BBU instability can be classified into two major categories, regenerative and cumulative. In the regenerative BBU, upstream (backward) propagation of the nonaxially symmetric mode provides feedback for amplification within a single accelerator section.[2] In the cumulative (also called multisection) BBU instability, the nonaxially symmetric modes of different accelerator sections are coupled only by the passage of the electron beam. The study presented in this paper will deal exclusively with the cumulative BBU. The BBU is capable of growing over time in one cavity as the trailing portions of the beam become more severely deflected than the proceeding portions. This instability can also grow over distance as the amplifying disturbances are carried along the beam, resulting in a range of macroscopic effects, from simple degradation of beam quality (emittance growth) to total loss of beam current if the beam strikes the cavity walls. BBU therefore places a limit on the beam's pulse length, propagation distance, and the beam current.

Despite the serious limitations imposed on accelerators by the BBU, there have been few publications where BBU is systematically studied in experiments and compared with the theories. The goal of the experiments presented in this paper is to systematically study the experimental scaling laws and growth rates for the BBU instability. With this goal in mind, the experimenter is free to investigate parameters that have limited variability in large scale accelerator programs. These parameters include beam current, focusing magnetic field, pulse lengths, cavity Q, and BBU frequency. This work then is the first experiment designed whose sole objective is to investigate the behavior of the BBU. A summary of some of these University of Michigan experiments can be found in Ref. 3. A second objective is to develop novel techniques to reduce the growth of the BBU. One such technique performed during the course of this research is the demonstrated use of "external cavity coupling."[4]

The experimental approach proceeded in three phases. The first experiments examined the growth of the BBU using an approximately 1 m long array of rf resonant pillbox cavities characterized by relatively high $Q(\approx 1000)$ and moderately large frequency spread $(\Delta f/f_0 \approx 0.1\%)$ among the cavities. These high Q experiments demonstrate the importance of beam loading. To reduce the effects of beam loading, in the next phase, a cavity array with a lower Q was employed (≈ 200), but the frequency spread was much smaller $(\Delta f/f_0 \approx 0.03\%)$. Two subsets of these latter experiments were performed, investigating BBU behavior over beam propagation distances of 1 and 2 m. The

[a]Present address: Sandia National Laboratories, Dept. 1231, Albuquerque, NM 87185.
[b]Present address: Synchrotron Radiation Center, University of Wisconsin–Madison, Stoughton, WI 53589-3097.

 B-1 0021-8979/94/75(3)/1258/9/$6.00

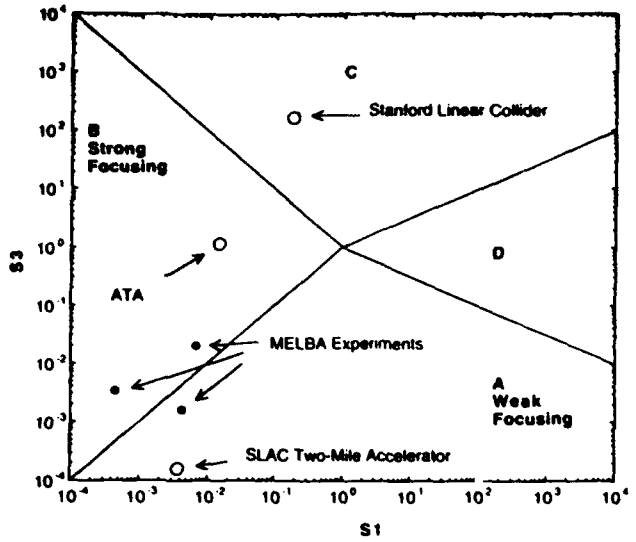

FIG. 1. Comparison of MELBA to other well-known accelerators in BBU growth rate parameter space (from Ref. 7).

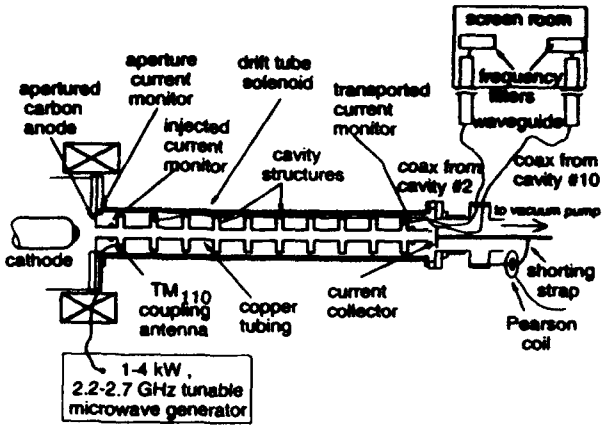

FIG. 2. Experimental configuration.

parameters for these experiments place the BBU growth rate scaling close to the boundary between the weak[1] and strong focusing[5,6] regimes (defined in Ref. 7). The third phase consisted of experiments designed to reduce the BBU growth rate using the aforementioned external cavity coupling.

The electron beam accelerator used in this research is the Michigan Electron Long Beam Accelerator (MELBA).[8] A useful comparison of MELBA growth rate scalings to those of other well-known accelerators is shown in Fig. 1. As explained in Ref. 7, the parameter $S1$ is proportional to beam current, and inversely proportional to the square of the applied focusing field, and $S3$ is the ratio of accelerator length normalized by the betatron wavelength to the pulse length normalized by the period of the deflecting mode. Each region on the graph represents a unique BBU growth rate scaling defined in Ref. 7.

II. HIGH Q LARGE FREQUENCY SPREAD EXPERIMENTS

The MELBA diode operates with the following parameters: voltage $=-0.7$ to -0.8 MV, diode current $=1$–10 kA, and pulse length $=0.3$–5 μs, with flattop voltage provided by an Abramyan-type compensation stage over 1 μs.

The experimental configuration is shown in Fig. 2. The electron beam is generated from an explosive emission velvet cathode. This cathode consists of a glyptal-coated hemispherical-end cathode stalk with a velvet emitting button attached to the end of the cathode stalk. This cathode is advantageous for its slow diode closure, limited edge emission, and relatively long glyptal life. The anode is a graphite plate (1/8 in. thick) located 10.8 cm from the end of the cathode. A circular aperture with a diameter of 2 cm is centered on the anode plate to extract 40–300 A into the transport chamber.

The diode chamber is immersed in a solenoidal magnetic field that can be varied from 0.5 to 1.2 kG. The transport chamber is composed of a 1 m long drift tube surrounded by solenoid coils pulsed independently from the diode. The current to the solenoid is provided by a two-stage, double-polarity, electrolytic capacitor bank that produces a magnetic field up to 3.5 kG. Since the diode coils and the drift tube solenoid overlap, the superposition of the solenoidal fields causes a total B-field profile that is not quite uniform in the experimental chamber. The profile is higher on the upstream end before tapering to a flattop about halfway down the drift tube.

Within the drift tube are ten brass pillbox resonant cavities separated by smaller diameter copper tubes. Each cavity has a radius of 6.9 cm and a length of 2.0 cm. Within each cavity is a small loop antenna oriented to be sensitive to the TM_{110} cavity mode. With cylindrical pillbox cavities, the TM_{110} mode is the most significant BBU mode, because it is the fundamental, nonaxially symmetric TM mode, and it produces the maximum instability growth. The length of the separation tubes is 6.5 cm, giving an intercavity distance of 8.5 cm. The diameter of the tubes is 3.8 cm, which is below the TM_{010} cutoff diameter, and thus serves to isolate each cavity from rf crosstalk. The measured attenuation of the $\approx$2.5 GHz, TM_{110} mode microwaves is 26 dB from cavity to adjacent cavity. This ensures that the BBU under study is the cumulative type (i.e., nonregenerative type).

The first cavity (closest to the anode) has its TM_{110} mode primed externally by an Epsco (model PG5KB) microwave pulse generator. The priming microwave pulse is generally 3 μs long and begins before the e-beam is present. The power of the injected microwaves is generally 1 kW. The purpose of this procedure is to provide sufficient initial transverse modulation to the beam to allow BBU growth in a ten cavity system.

The general technique used in these experiments is to investigate the BBU instability by taking measurements on the characteristic microwaves produced by the instability. In particular the magnitude of BBU growth is determined through the growth of the TM_{110} microwave power between the second and tenth cavities.

In the second cavity the e-beam-induced rf is measured

TABLE I. Parameters for high Q, large frequency spread cavities.

Cavity No.	TM_{110} resonant frequency (GHz)	TM_{110} Q
1	2.5190	660
2	2.5200	1090
3	2.5200	1420
4	2.5201	1800
5	2.5265	530
6	2.5270	680
7	2.5230	1160
8	2.5240	920
9	2.5248	680
10	2.5250	1010
Average	2.5230±0.1%	1000±310

via the loop antenna. The microwaves are propagated out of the experimental chamber through RG/0.405 U semi-rigid transmission cable to a vacuum feedthrough, to RG/8 cable, to an S-band waveguide. The waveguide runs to a Faraday cage where the signal is attenuated and filtered for frequency information. Part of the microwave signal is diverted into a filter that passes 2.523 GHz±11 MHz. This frequency, as noted above, corresponds to the TM_{110} BBU frequency.

The rf power in the tenth (last) cavity is measured in the same way with its own set of cables and waveguides. The growth of the BBU instability is determined by the decibels of growth in 2.5 GHz microwave power between the second and tenth cavities.

Electron beam current is measured at several points in the transport experiment. Cathode stalk current in the diode is measured by a B-dot loop in the MELBA oil tank, behind the insulators. Extracted current is monitored by a Rogowski coil in the flange after the anode. Injected current is measured by a Rogowski coil before the first cavity and exit current is detected by a Rogowski coil after the last cavity. Exiting current is also measured by a carbon plate/current collector which is grounded by a strap which passes through a Pearson current transformer.

The exact TM_{110} resonant characteristics of the ten cavities in the transport array are listed in Table I. The cavities are numbered in order of beam encounter. As indicated, the average resonant frequency is 2.523 GHz ±0.1%, and the average Q is 1000±310. Comparison of the frequency spread ($\Delta f/f_0$=0.1%) and average resonant linewidth ($1/Q$=0.1%) reveals that they are approximately equal, and thus the frequency spread among the cavities can be referred to as large.

Figure 3 shows a typical data set of electron beam and rf signals from a high Q, large-frequency-spread BBU transport experiment. The uppermost signal trace (a) is the voltage applied to the diode by the MELBA Marx generator. The voltage has a total length of about 700 ns and the duration of the flattop is about 400 ns. The voltage magnitude at the flattop is −750 kV. The second trace (b) is the signal from the Rogowski coil that encircles the entrance to the first cavity. This signal has a flattop amplitude

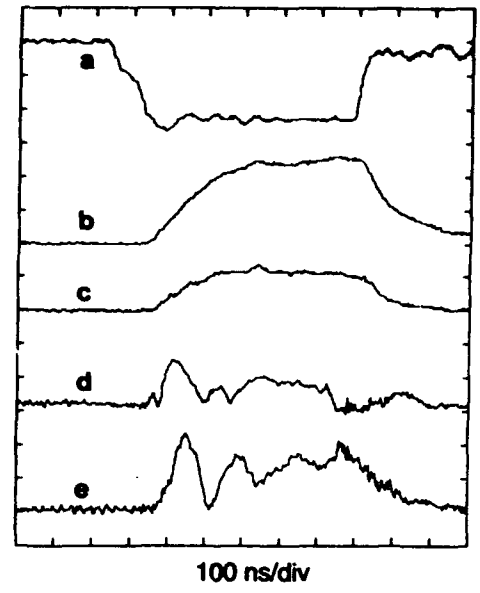

FIG. 3. Experimental data taken from two similar shots. (a) Diode voltage (310 kV/div), flattop is 750 kV. (b) Injected current (92 A/div), maximum is 230 A. (c) Transported current (40 A/div), flattop is 46 A. (d) Detector signal of second cavity rf (100 mV/div), signal attenuated by 12 dB. (e) Detector signal of tenth cavity rf (100 mV/div), signal attenuated by 32 dB. Time scale is 100 ns/div. Solenoidal magnetic field is 1.1 kG.

corresponding to approximately 220 A. The center trace (c) represents the transported current. This trace is the signal from the Pearson coil that surrounds the cable which connects the collector plate to ground. The magnitude of beam current on the flattop for this signal is 46 A. The drift tube solenoid produced a magnetic field of 1100 G for this particular shot. The fourth trace (d) is the diode crystal detector signal of the microwaves picked up by the loop antenna in the second cavity. This signal has passed through the frequency filter which passes frequencies at 2.523±0.011 GHz. The external attenuation added to the second-cavity microwaves is 12 dB. The lowermost trace (e) is the microwave crystal detector signal as received by the loop antenna in the tenth (last) cavity; this signal has passed through a frequency filter similar to that used for the second-cavity diagnostics. The external attenuation added for this signal is 32 dB. The external microwave priming source was tuned to the exact resonance of the first cavity (see Table I), 2.519 GHz, and the power of the priming pulse was approximately 1 kW.

The experimental spatial growth rate for the BBU instability can be determined from the data presented in Fig. 3. The experimental growth rate is ascertained through examination of the rf signals [traces (d) and (e) from Fig. 3]. These traces are diode crystal detector signals which give measurements of microwave power injected into the detectors. Scrutiny of the microwaves from the second cavity [signal (d) of Fig. 3] shows a detector signal of about 80 mV along the flattop of the MELBA voltage pulse. A signal magnitude of 80 mV corresponds to a power of 9 mW for this particular detector. Before entering the detector, the signal was purposely reduced by 12 dB in external

attenuation and also by another 2.7 dB from resistive and insertion losses in the cable, waveguide, and frequency filter. Thus, the total power of the TM_{110} microwaves on the flattop picked up by the loop antenna in the second cavity is 270 mW.

The TM_{110} microwave signal in the tenth cavity has a magnitude of about 160 mV on the flattop. Note that the overall shape of the tenth-cavity microwave power is similar to that of the second cavity. There is about 40 ns of delay between the tenth and second cavity signals due to a longer waveguide used to transport the microwaves from the tenth cavity. This suggests that the magnitude of the microwaves in the tenth cavity is a direct result of growth from the second-cavity microwaves. This detector's calibration at 160 mV gives a detector power of 35 mW. The added attenuation in this signal is 32 dB with an additional reduction of 2.9 dB from resistive and insertion losses. Thus, the total power received by the antenna in the tenth cavity is 99 W. Therefore, the growth in TM_{110} microwave power between the second and tenth cavities as sampled by the loop antennas is 99 W/0.27 W$\approx$370, which is equivalent to 26 dB. The distance between the antennas is 68 cm, giving a spatial microwave growth rate of 38 dB/m.

A theoretical prediction for the amount of BBU growth can be found using the continuum dispersion relation[7,9,10] for solenoidal focusing:[11]

$$(\Omega^2-\omega_c\Omega+\Gamma)(\Omega^2+\omega_c\Omega+\Gamma)=0, \tag{1}$$

where $\Omega=\omega-kv$ and

$$\Gamma=\frac{2\omega_0^4\epsilon}{-\omega^2+\omega_0^2+i\omega\omega_0/Q}.$$

The variable k is the wave number of the instability, ω is the frequency which undergoes BBU growth, ω_0 is the TM_{110} angular resonant frequency, v is the electron beam velocity, Q is the cavity quality factor, ω_c is the relativistic angular betatron frequency, and ϵ is the dimensionless coupling constant,[7] where

$$\epsilon=0.422\frac{l}{L}\frac{I}{17kA}\frac{\beta}{\gamma}.$$

Here, l is the cavity length, L is the spacing of cavity centers, I is the e-beam current, and β and γ have their usual meanings. For the experimental parameters of $l=2$ cm, $L=8.5$ cm, transported current=46 A, and kinetic energy=750 keV, one finds $\epsilon=1.0\times10^{-4}$. A solenoidal field of 1.1 kG yields $\omega_c=7.85$ Grad/s, the BBU frequency is the priming frequency, $\omega=2\pi\times2.519$ GHz, and the average TM_{110} frequency is $\omega_0=2\pi\times2.523$ GHz. Insertion of these values into Eq. (1) produces a theoretical spatial growth rate in the continuum model of

$$\mathrm{Im}(k)=4.90\ \mathrm{m}^{-1}.$$

Thus, the e-folding length for the instability is 20.4 cm. This implies a rf amplitude growth over the 68 cm between the second and the tenth cavities of $\exp\{68.0/20.4\}=28.0$. An amplitude growth of 28 translates to 29 dB gain. Thus, the two-dimensional continuum theory predicts 29 dB of BBU growth for a 750 keV electron beam with current=46 A, and a solenoidal focusing field of 1.1 kG. This is in reasonably good agreement with the experimental growth of 26 dB, considering the use of a continuous model for the few cavity system and the neglect of beam loading and frequency detuning among the cavities.

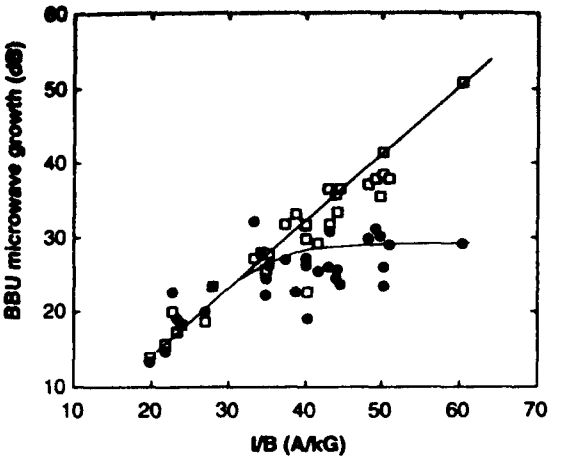

FIG. 4. Graph of beam breakup instability growth vs the ratio of transported current to magnetic field, I/B. For each point representing experimentally measured growth (closed circles), the corresponding theoretical prediction for growth using the same beam parameters is also plotted (open squares). The lines are guides for the eye.

The preceding continuum model treats the transverse impulsive forces from the accelerating cavities as a continuous force per unit length. This approximation limits the dispersion relations to the cases where instability scale lengths (i.e., e-folding length, and wavelength of the BBU disturbance) are long compared to the cavity spacing. Modeling the transverse force on the beam resulting from pillbox cavities placed at discrete locations produces the following dispersion relation:[11]

$$\cos\left(\frac{L\Omega}{v}\pm\frac{L\omega_c}{2v}\right)=\cos\frac{L\omega_c}{2v}+\frac{\Gamma L}{\omega_c v}\sin\frac{L\omega_c}{2v}. \tag{2}$$

The discrete cavity dispersion relation of Eq. (2) yields a prediction of 24 dB growth in the BBU, when the effect of frequency spread is taken into account, i.e., the growth in each cavity is computed locally using the individual parameters for each cavity (see Table I).

An unfortunate circumstance in this experiment is the fact that in order to increase the amount of transported current, the applied magnetic field must also be increased. Therefore, it is difficult to determine the scaling of the BBU growth versus current while holding the magnitude of the focusing field constant or vice versa. An attempt to incorporate the I vs B dependence into the growth rate analysis examines the BBU growth rate versus the ratio of current to magnetic field, I/B. Figure 4 plots the experimental and theoretical growth of the BBU vs I/B using the two-dimensional continuum theory, Eq. (1).

In Fig. 4, it is evident that the BBU growth predicted by continuum theory (open squares) agrees well with BBU growth in experiments with low I/B. For large values of

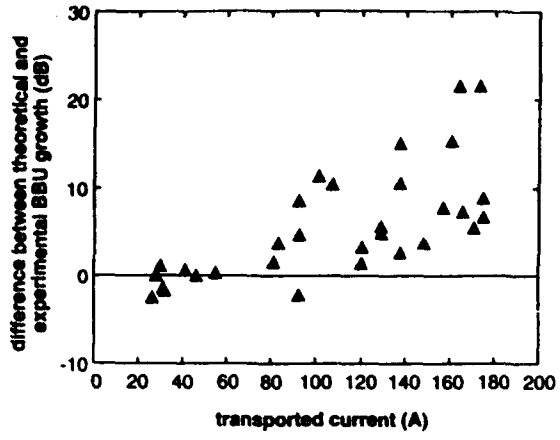

FIG. 5. Graph showing the difference between theoretically computed and experimentally observed BBU growth (i.e., $\Gamma_{theory}-\Gamma_{experiment}$) vs transported beam current. Horizontal line shows position of exact agreement.

I/B, however, there is significant divergence between theory and experiment. Application of the discrete cavity theory, Eq. (2), does not provide much better agreement. An explanation for this difference between theory and observation could be "beam loading," which changes the electromagnetic properties of a cavity by the presence of an e-beam. One effect of beam loading is to shift the resonant frequency for a beam-filled cavity according to[12]

$$\omega_0' = \sqrt{\omega_0^2+\omega_{pe}^2} \tag{3}$$

where ω_0' is the corrected upshifted resonant frequency, ω_0 is the angular resonant frequency of the cold cavity, and ω_{pe} is the angular plasma frequency of the electron beam given by

$$\omega_{pe}^2 = \frac{4I_b c^2}{r_w^2(17\text{ kA})}\sqrt{\frac{1+\alpha^2}{\gamma^2-1}}, \tag{4}$$

where I_b is the beam current, r_w is the radius of the cavity, and α is the perpendicular to parallel electron velocity ratio. For example, an electron beam with parameters: $I_b=100$ A, $V=750$ kV, $r_w=6.9$ cm, and $\alpha=0.1$, and $\omega_0=2\pi\times2.523$ GHz, the corrected angular resonant frequency is $\omega_0'=2\pi\times2.524$ GHz. This increase may seem slight, but it is important to remember that the cavities have a high Q (narrow linewidth). For $I_b=128$ A the resonance of the average cavity is shifted 0.05%. This shift is equal to the linewidth of a cavity with $Q=1000$.

In other words, if the current is high enough, then the beam can "detune" the cavities with respect to the beam modulation-cavity resonance condition which drives the BBU. The effect of this shift is that the frequency of the BBU disturbance (equal to the priming frequency) is too low to drive the (detuned) TM_{110} mode, leading to the observed reduction of BBU growth in the experiments.

Figure 5 shows the difference between the predicted magnitude of BBU growth from continuum theory and the observed growth ($\Gamma_{theory}-\Gamma_{experiment}$) versus transported current. The larger discrepancy at higher beam current is strong evidence for the beam loading effect. It is also interesting to note that significant difference appears to begin at approximately 100 A, which is where the frequency upshift is comparable to the linewidth of the average cavity.

In order to gain further understanding of the detuning phenomenon and its effect on the BBU growth rate, experiments in which the priming frequency was changed were carried out. These experiments could be considered as the converse of beam loading. Beam loading causes the resonant frequencies of the cavities to be detuned with respect to the frequency of the beam modulation. Changing the priming frequency, however, causes the beam modulation to be altered with respect to the cavity resonant frequencies. For these experiments the beam current is kept low (<50 A) so that the beam loading effect is slight. An advantage in this case is that the priming frequency can be very accurately determined, whereas detuning through beam loading is ambiguous because of uncertainties in the exact frequency upshift due to the beam only partially filling the cavity, and differences in Q's and variations in resonant frequencies among the cavities.

When the priming microwaves are turned off, very little signal is observed on the crystal detectors, indicating undetectable instability growth arising from noise over the ten cavities. This suggests that the frequency of modulation applied to the beam through priming will be the dominant frequency available for BBU growth. In other words, the effect of priming is so strong that growth at any any other frequency will be small compared to the BBU growth of the priming microwaves. This feature has the additional advantage of observing BBU growth at a frequency other than the exact resonant frequency.

A summary of microwave growth for several shots taken over a range of priming frequencies is shown in Fig. 6. The currents for these data range from 40 to 50 A and the applied magnetic field for all shots is 1.1 kG. Superimposed on the data are the dispersion relations, $\mathrm{Im}(k)$, from the continuum theory Eq. (1) (thin lined curve), and the discrete cavity theory, Eq. (2) (thick lined curve), with ω equal to the priming frequency. The continuum theory uses ω_0 equal to the average cavity TM_{110} resonant frequency of 2.523 GHz and thus neglects frequency spread. The discrete cavity theory is the sum of predicted growths resulting from each cavity using each cavity's own ω_0 and Q. The peaking of the data near the average TM_{110} resonant frequency is evidence that the BBU instability is indeed responsible for the observed microwave growth. The data also trace a broader curve than the continuum theory. This feature is due to the resonant frequency spread among the cavities in the array. The initial cavity's TM_{110} resonant frequency is 2.519 GHz. Thus, the TM_{110} fields are strongest and produce the most initial beam modulation when the priming is tuned to 2.519 GHz. In the region of 2.519–2.524 GHz, both the data and the discrete cavity theory indicate nearly constant growth rate. Intuitively, this constant region exists because near 2.519 GHz, cavities 1–4 should show near maximum growth, but cavities 5–10 should exhibit decreased growth. At 2.524 GHz the situation is reversed. Beyond 2.524 GHz the microwave growth

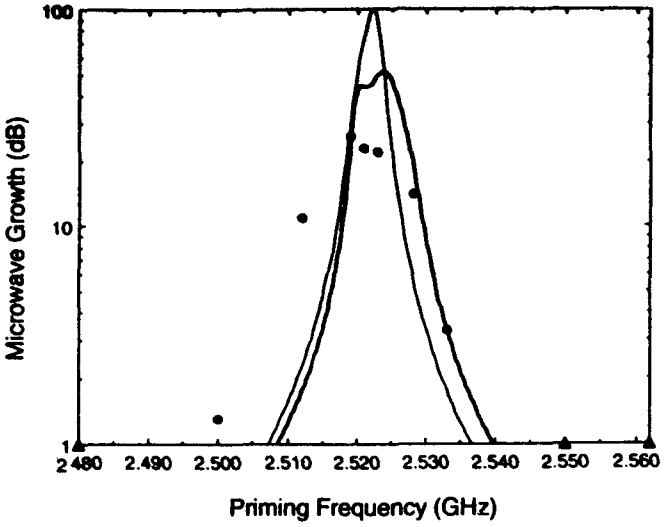

FIG. 6. Microwave growth vs priming frequency. Experimentally observed microwave growth (closed circles) is shown with the theoretical growth curves for I_b=45 A and B=1.1 kG. The thick lined curve is the predicted growth from the discrete cavity theory [Eq. (2)], and the thin lined curve uses the continuum theory which does not include frequency spread. The closed triangles along the abscissa represent experimental growth below the level of detectability.

diminishes rapidly following the theoretical curves.

The detuning experiments show that the coupling between the beam modulation and cavity fields is strongly dependent upon the resonant condition. The theory has proven accurate at low currents, but at high currents the experiments are not adequately explained by the existing theory partly because of beam loading and partly because of the significant spread in the resonant frequencies. Some obvious improvements to this situation are apparent. One improvement would be to accurately match ($\ll$0.1%) the TM_{110} resonant frequencies. Especially important would be to match the frequency of the initial priming cavity to the average resonant frequency. This motivated our lowering of the Q's of the cavities, the result of which is reported next.

III. LOW Q, SMALL FREQUENCY SPREAD EXPERIMENTS

In an attempt to create a fair test between theory and experiment that would be valid at high e-beam currents, the cavity array was modified to a lower average Q, and a lower frequency spread. Table II lists the TM_{110} mode parameters for this second array. The Q lowering was achieved by inserting a thin annulus of microwave absorber (Eccosorb) into each cavity.

Low Q experiments using both 10 and 19 cavities have been performed. The BBU growth results with ten cavities have been published elsewhere (see Ref. 3), and they are included on the right-hand side of Fig. 7 for later comparison. Note that there is no significant deviation from theoretical growth at high values of I/B, indicating mitigation of the beam loading effect.

TABLE II. Parameters for low Q, small frequency spread cavities.

Cavity No.	TM_{110} resonant frequency (GHz)	TM_{110} Q
1	2.5070	230
2	2.5070	290
3	2.5060	215
4	2.5082	220
5	2.5070	280
6	2.5072	230
7	2.5076	160
8	2.5078	185
9	2.5085	180
10	2.5086	170
Average	2.5075±0.03%	215±45

Experiments using an additional 9 cavities, for a total of 19, have been recently performed. A longer (2 m) solenoidal drift tube was employed, but otherwise the configuration and diagnostics are similar to those of the 10 cavity experiments (shown in Fig. 2). The parameters for the additional nine cavities (11–19) are shown in Table III.

The left-hand portion of Fig. 7 illustrates the BBU growth versus I/B for the 19-cavity system. The lower I/B values for the 19-cavity experiment are due to the lower magnetic field and thus lower transported current capable of being generated by the 2 m solenoid. For each experimental datum the corresponding discrete-cavity theoretical growth is also plotted. Note that the slope of the growth for the 10-cavity case is approximately half of that for the 19-cavity case, as expected.

Experimental data were also taken to gain information about the dispersion relation when $\omega \neq \omega_0$ for the 10-cavity case and is shown in Fig. 8. Just as in the high Q, large frequency spread experiments, the priming frequency was varied about the resonant frequency. This set of experi-

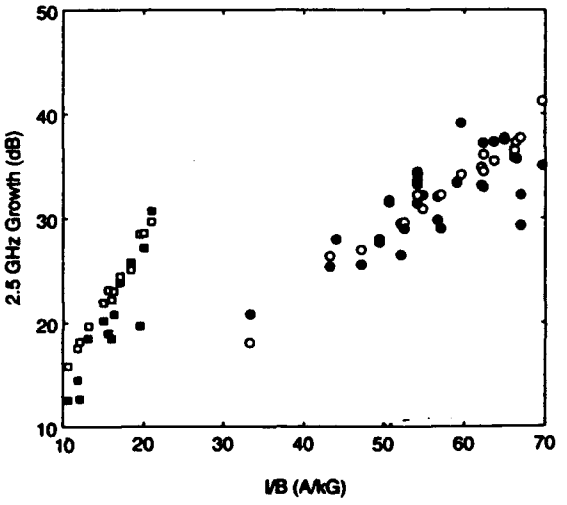

FIG. 7. BBU growth (dB) vs ratio of beam current to magnetic field, I/B (A/kG). Experimental data (closed symbols) are plotted with corresponding theoretical growth (open symbols). Two experimental cases are shown: 19 cavities (squares) and 10 cavities (circles).

B-6

TABLE III. Parameters for additional cavities in the 19 cavity experiment.

Cavity No.	TM_{110} resonant frequency (GHz)	TM_{110} Q
11	2.5070	290
12	2.5079	250
13	2.5070	260
14	2.5073	300
15	2.5075	230
16	2.5076	190
17	2.5082	160
18	2.5085	300
19	2.5080	270
19 cavity average	2.5076±0.03%	230±45

ments was also presented in Ref. 3, but is reproduced here for a ready comparison with Fig. 6 (high Q experimental results). The plotted points (filled circles) are experimental data taken at the same magnetic field (3.4 kG) and nearly the same e-beam current (190–215 A). The thick-lined curve is the BBU growth as predicted by the discrete-cavity Eq. (2) using $I=210$ A, and using each cavity's specific resonant frequency and Q. The thin-lined curve is the continuum BBU growth Eq. (1) for the same parameters, but uses the average ω_0 of $2\pi\times2.5075$ GHz and the average Q of 215. Note that the data follow the discrete cavity theory more closely in this case than in Fig. 6.

IV. BBU REDUCTION USING EXTERNAL CAVITY COUPLING

A. Experimental results

The purpose of the experimental program described in this paper is twofold. The first objective of this research was to successfully describe the behavior of the BBU instability by building an experiment specifically designed to study the BBU growth in a controlled manner. The results of the 10-cavity low Q, small frequency spread experiments detailed above and in Ref. 3 provide a good basis for pursuit of the next goal. The second intent of these experiments is to develop novel techniques for suppression of the BBU. In the high Q, large frequency spread case, BBU was reduced by beam loading and by breakup mode frequency variations. The knowledge that these effects can reduce BBU growth rates is not particularly novel. The use of rf cures, especially by stagger tuning, has been studied elsewhere,[2,10,13–16] although it was beneficial to confirm BBU growth reduction through these mechanisms.

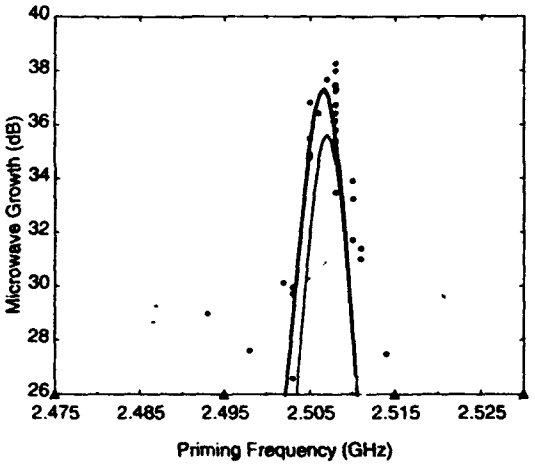

FIG. 8. Microwave growth dependence on the frequency of priming microwaves. Experimental data are represented by the closed circles. The thicker curve is the theoretical growth predicted by the discrete-cavity theory. The thinner curve is the theoretical growth predicted by the continuum theory. The triangles along the abscissa indicate experimental growth below the level of detectability (from Ref. 3).

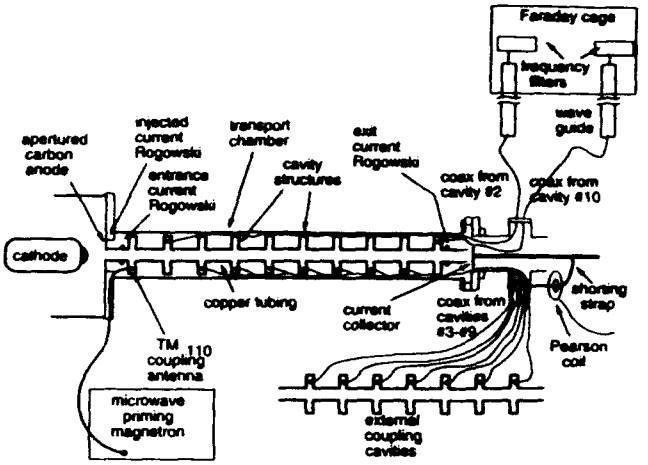

FIG. 9. External coupled cavity configuration.

A notably novel mechanism for BBU reduction has been suggested theoretically by Colombant, Lau, and Chernin[17] and is particularly capable of being tested by the MELBA experiments. This method has been termed "external cavity coupling," and the initial experimental results using this method are detailed in Ref. 4. In this method the main beam cavities are coupled by transmission line to identical external dummy cavities on the outside of the transport structure. The idea here is that the beam cavities are capable of "sharing" deflecting mode energy with the dummy cavities and thus reduce the magnitude of the TM_{110} mode fields in the beam cavities, with subsequent reduction in the BBU growth rate.[18,19] The 10-cavity MELBA experimental configuration is readily adaptable to this method, since each cavity contains a coupling loop antenna to sample the TM_{110} microwaves. Each antenna can be connected to a coaxial cable to transmit the microwaves out of the cavity. In this way, the loop antennas can double as a microwave sampler and as a device to deliver the TM_{110} mode energy to a dummy cavity containing a similar coupling loop.

Figure 9 shows the experimental configuration used for the external cavity coupling experiments. This arrangement is almost identical to the configuration used for the low Q, small frequency spread baseline growth experiments described in Sec. III. The difference is that the seven intermediate cavities (3–9) between the second and tenth have

B-7

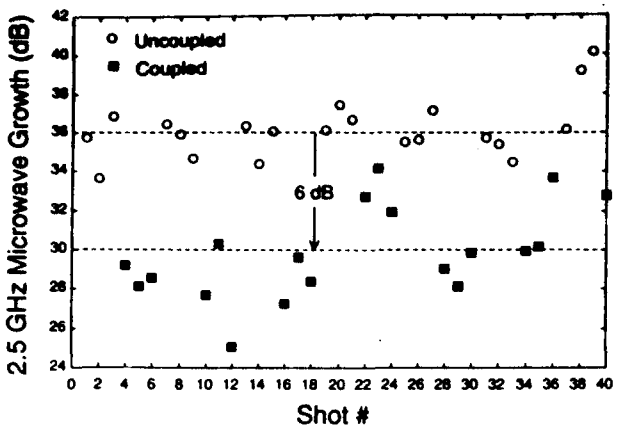

FIG. 10. Growth (dB) of the BBU microwave power for 40 different electron beam pulses showing uncoupled shots (open circles) and externally coupled shots (closed squares) (from Ref. 4).

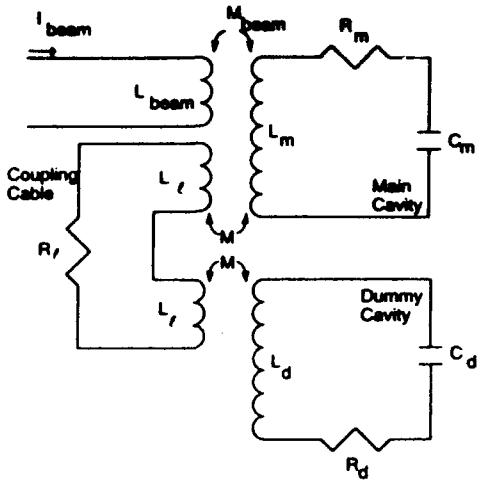

FIG. 11. Equivalent circuit representing the coupled cavities in the actual experimental configuration.

their coupling loops connected via microwave cable to seven nearly identical cavities located externally to the solenoid drift tube. The length of this cable was chosen to be 16 wavelengths long. Typically an experimental run alternated between a few shots with the internal and external cavities coupled (loop antennas connected), followed by a few shots with the internal and external cavities uncoupled. When the cavities are uncoupled, the experiment is equivalent to the baseline low Q, large frequency spread BBU growth experiments described above.

A summary of BBU microwave growth data from some 40 shots (from Ref. 4) is presented in Fig. 10. The data show a consistent reduction of BBU growth from an average of 36 dB ($\sigma = \pm 1.5$ dB) for the uncoupled case to an average of 30 dB ($\sigma = \pm 2.4$ dB) for the coupled-cavity case. Thus, an average reduction in the BBU of 6 dB is measured for this system in which seven internal beam cavities are coupled to a nearly identical set of seven external dummy cavities.[4]

B. Coupling constant, κ, determination

Previous analysis[4] has shown that the BBU spatial growth rate, Γ (where total BBU growth is given by $e^{\Gamma z}$), is modified by a factor of $1/(1+\kappa^2 Q^2)$ to account for cavity coupling through a simple one-dimensional mutual inductance model.[17–19] Thus, the external coupled cavity growth rate is $\Gamma/(1+\kappa^2 Q^2)$. Here, κ is the coupling constant and Q is the cavity quality. This factor of $\kappa^2 Q^2$ represents the ratio of power leaked to the dummy (external) cavity to the power remaining in the main (internal) cavity.[4] A cold test was performed on a network analyzer (HP-8510) using two model cavities each with two coupling antennas. One antenna in each cavity was used to inject the microwaves and the second was used to transmit the rf power out of the cavity. This cold test experiment indicated that the power sharing ratio for this arrangement is $\kappa^2 Q^2 = 0.13$. Using this value in the reduction factor yields an expected experimental reduction to 36 dB(1/1.13) $\approx$ 32 dB.

However, the cold test of the power sharing ratio differs from the actual experimental configuration. In the experiment, each cavity has only one coupling loop, thus the cold test may underestimate the magnitude of power sharing since the extra antennas provide additional inductance to the overall circuit. An alternative method to determine κ has been developed using an equivalent circuit model similar to those used in coupled cavity klystron analyses.[20] The equivalent circuit representing the experimental configuration is shown in Fig. 11. The critical parameter that governs the magnitude of power sharing is the mutual inductance, M, connecting the loop antenna circuits to the cavity circuits. The mutual inductance can be found from the formula:[21,22]

$$\frac{\omega_0^2 M^2}{R} = \frac{2s^2 J_1^2(3.83r/b)Q}{J_0^2(3.83)\epsilon_0 r^2 \pi b^2 l Z_0 \omega_0}, \tag{5}$$

where ω_0 is the angular TM_{110} resonant frequency, R is the resistance assigned to the cavity circuit, s is the area of the coupling loop, r is the radial position of the antenna in the cavity, b is the radius of the cavity, l is the cavity length, and Z_0 is the characteristic impedance of the coupling cable. Table IV lists the circuit parameters shown in Fig. 11. Solving for power in the main and dummy cavities with the circuit program SPICE[23] yields a power sharing ratio of $\kappa^2 Q^2 = 0.18$. Use of this value in the $1/(1+\kappa^2 Q^2)$ reduction factor gives a predicted value of 30 dB growth for the

TABLE IV. Values of equivalent circuit components.

Component	Symbol	Value
Capacitance of cavities	C_m, C_d	29.6 fF
Inductance of cavities	L_m, L_d	137 nH
Resistance of cavities	R_m, R_d	10 Ω
Inductance of coupling loop	L_l	6.4 nH
Resistance of coupling loop	R_l	0.01 Ω
Mutual inductance between loop and cavity	M	2.7 nH

B-8

coupled cavity experiments. This results in better agreement between theory and experiment than that reported in Ref. 4.

It might be argued that cavity coupling is equivalent to the often used BBU reduction technique of Q lowering, because both methods serve to lower the strength of the TM_{110} mode fields. There is a significant difference, however. A finite Q represents lossy processes from which energy cannot be recovered, whereas a nonzero κ represents only reactive loading which does not result in any energy loss. If Q were set to infinity, i.e., no dissipative losses, the process of power sharing would still exist and BBU growth rate reduction would still occur.[17] Therefore, this technique provides a novel way in which to reduce the adverse effects of the BBU instability.

V. CONCLUSIONS

This paper contains the results of an experimental program whose only goal is to investigate the behavior of the BBU instability. Through the course of this research several original developments have been made regarding the physics of the BBU instability. The use of the continuum model was shown to accurately predict the growth of the BBU in a few (10) cavity system. The use of a more realistic discrete cavity model gave slightly better agreement. The importance of beam loading at high e-beam currents was demonstrated. Experimental BBU growth at increased current was found to be less than in theories (which do not include beam loading). The beam loading effect was mitigated when a cavity array employing lower Q's and lower frequency spread was used. Increasing the e-beam propagation distance had the expected effect on the BBU growth rate (increasing the slope of the growth vs current curve). The use of external cavity coupling as a novel BBU reduction technique was demonstrated, resulting in a 0.75 dB reduction per cavity. A model implementing power sharing through mutual inductance is capable of explaining the reduction with excellent agreement.

ACKNOWLEDGMENTS

This research was supported by Strategic Defense Initiative Office of Innovative Science and Technology managed by the Office of Naval Research. Support for P.R.M. was also supplied by a Rackham School of Graduate Studies Fellowship. Experimental assistance from M. T. Walter and C. H. Ching is acknowledged and appreciated.

[1] W. K. H. Panofsky and M. Bander, Rev. Sci. Instrum. **39**, 206 (1968); A. W. Chao, B. Richter, and C. Y. Yao, Nuc. Instrum. Methods **178**, 1 (1980).

[2] R. Helm and G. Loew, in *Linear Accelerators*, edited by P. M. Lapostelle and A. L. Septier (North-Holland, Amsterdam, 1970), Chap. B. 1.4, p. 173; A. W. Chao, *Physics of Collective Beam Instabilities in High Energy Accelerators* (Wiley, New York, 1993), p. 136.

[3] P. R. Menge, R. M. Gilgenbach, and R. A. Bosch, Appl. Phys. Lett. **61**, 642 (1992).

[4] P. R. Menge, R. M. Gilgenbach, and Y. Y. Lau, Phys. Rev. Lett. **69**, 2372 (1992).

[5] V. K. Neil, L. S. Hall, and R. K. Cooper, Part. Accel. **9**, 213 (1979).

[6] G. J. Caporaso, F. Rainer, W. E. Martin, D. S. Prono, and A. G. Cole, Phys. Rev. Lett. **57**, 1591 (1986).

[7] Y. Y. Lau, Phys. Rev. Lett. **63**, (11), 1141, 2433E (1989).

[8] R. M. Gilgenbach, L. D. Horton, R. F. Lucey, Jr., S. Bidwell, M. Cuneo, J. Miller, and L. Smutek, in *Digest of the 5th IEEE Pulsed Power Conference* (IEEE, New York, 1985), p. 126.

[9] V. K. Neil and R. K. Cooper, Part. Accel. **1**, 111 (1970).

[10] D. G. Colombant and Y. Y. Lau, Appl. Phys. Lett. **55**, 27 (1989).

[11] R. A. Bosch, P. R. Menge, and R. M. Gilgenbach, J. Appl. Phys.**71**, 3091 (1992).

[12] R. E. Shefer and G. Bekefi, Int. J. Electron. **51**, 569 (1981).

[13] R. L. Gluckstern, F. Neri, and R. K. Cooper, Part. Accel. **23**, 37 (1988).

[14] D. Chernin and A. Mondelli, Part. Accel. **24**, 177 (1989).

[15] K. A. Thompson and R. D. Ruth, Phys. Rev. D **41**, 964 (1990); R. H. Miller *et al.*, SLAC Pub. 5862, 1992.

[16] C. L. Bohn and J. R. Delayen, Phys. Rev. A **25**, 5964 (1992).

[17] D. Colombant, Y. Y. Lau, and D. Chernin, Part. Accel. **35**, 193 (1991).

[18] D. G. Colombant and Y. Y. Lau, J. Appl. Phys. **72**, 3874 (1992).

[19] D. G. Colombant and Y. Y. Lau, Nuc. Instrum. Methods A **311**, 1 (1992).

[20] R. E. Collin, *Foundations for Microwave Engineering* (McGraw–Hill, New York, 1966), Chaps. 7 and 9.

[21] R. A. Bosch, P. R. Menge, and R. M. Gilgenbach (unpublished).

[22] P. R. Menge, Ph.D. dissertation, The University of Michigan, 1993.

[23] P. W. Tuinenga, *SPICE, A Guide to Circuit Simulation and Analysis Using PSpice* (Prentice–Hall, Englewood Cliffs, NJ, 1988).

Beam breakup instability in an annular electron beam

Y. Y. Lau and John W. Luginsland
Intense Energy Beam Interaction Laboratory and Department of Nuclear Engineering, University of Michigan, Ann Arbor, Michigan 48109-2104

(Received 8 March 1993; accepted for publication 19 July 1993)

It is shown that an annular electron beam may carry six times as much current as a pencil beam for the same beam breakup (BBU) growth. This finding suggests that the rf magnetic field of the breakup mode is far more important than the rf electric field in the excitation of BBU. A proof-of-principle experiment is suggested, and the implications explored.

Annular electron beams have the capability of carrying a much higher current than a pencil beam. Besides the obvious fact that annular beams have a larger cross-sectional area, their limiting currents are significantly higher than those of a pencil beam when placed in a metallic drift tube. For this and other reasons, annular beams have recently been chosen as the preferred geometry to generate coherent, ultrahigh power microwaves.[1,2] They have also been used as the primary beam in several "two-beam accelerator" configurations.[3,4] These annular beams either encounter a sequence of modulating gaps, or simply glaze by a slow wave structure to generate a wake field in the case of two-beam accelerators.[3] The beam radius, the pill box radius, and the slow wave structure radius may all be of the same order of magnitude. The high current would then lead to the beam breakup instability (BBU)[5-8] and this concern motivates the present study.

BBU is usually analyzed for a pencil beam propagating along the center axis of a sequence of accelerating cavities. Many BBU calculations of practical interest assume that the accelerating unit is the familiar cylindrical pillbox cavity and that the dominant deflecting mode is the TM_{110} mode.[5,6,10] Extension to an annular beam is straightforward. Nevertheless, this calculation leads to several unexpected results and provides some new insights into BBU, to be reported in this communication.

It is well known that BBU is excited by the combined action of the rf magnetic field ($\mathbf{B}_1$) and the rf electric field ($\mathbf{E}_1$) of the deflecting modes:[5] $\mathbf{B}_1$ causes beam deflection through the Lorentz force and $\mathbf{E}_1$ causes mode amplification through the work done on the mode by the beam current $\mathbf{J}$. Our calculation strongly suggests that $\mathbf{B}_1$ is much more critical than $\mathbf{E}_1$ in contributing to BBU growth. Thus, an annular beam strategically placed near the minimum of the rf magnetic field would suffer far less beam breakup growth than a pencil beam that is centered on the cavity axis, where the magnetic field is large and the axial electric field is small. By the same argument, placing the annular beam very close to the wall of a metallic drift tube, at which the axial electric field is vanishingly small, cannot eliminate BBU growth because of the substantial deflecting magnetic field generated by the wall current. Toward the end of this communication, we propose an experiment which would unambiguously test the relative importance between the rf magnetic field and the rf axial electric field, as discussed here.

Consider an infinitesimally thin annular beam of radius r_0 inside a cylindrical pillbox of radius b. The beam carries a total current I and coasts at velocity v_0 with the corresponding relativistic factors γ and β. The drift tube is loaded with a slow wave structure, modeled by a series of cylindrical pillbox cavities, each of which supports the nonaxisymmetric TM_{110} mode.[3,5,6,10] The interaction between this mode and the beam causes BBU to be excited. In the limit $r_0 \to 0$, this is the basic model of BBU for a pencil beam. Since we are comparing the strength of BBU interaction for different values of r_0, we pretend that magnetic focusing is absent and that the quality factor Q of the deflecting mode is infinite.

Let $\mathbf{A}_1 = \hat{z} q(t)(\cos\theta) E(r)$ be the vector potential of the deflecting dipole mode in a cavity. For the fundamental TM_{110} mode, $E(r) = J_1(pr)$ represents the radial dependence of the axial electric field with J_1 being the Bessel function of order one and $p = 3.832/b$. The corresponding magnetic field is $\mathbf{B}_1 = \nabla \times \mathbf{A}_1$. The action of this mode on the beam is calculated as follows.

We divide the annular beam into N azimuthal segments (N large). The ith segment is located at $r = r_0$, $\theta = \theta_i = 2\pi i/N$, in the unperturbed state but is displaced radially by ξ_i and azimuthally by η_i when the deflecting mode is present. The linearized force law yields

$$-\gamma(\omega - kv_0)^2 \xi_i = (e/m_0)(v_0/c) q E'(r_0) \cos\theta_i, \tag{1}$$

$$-\gamma(\omega - kv_0)^2 \eta_i = -(e/m_0) \times (v_0/c) q [E(r_0)/r_0] \sin\theta_i, \tag{2}$$

where the right-hand sides represent the components of the Lorentz force that causes beam deflection. In writing Eqs. (1) and (2), we have assumed a wave-like solution $\exp[j(\omega t - kz)]$ for the disturbances, with $j^2 = -1$, and we have used a prime to denote derivative with respect to the argument.

The instantaneous current J on the ith current filament is

$$\mathbf{J}_i(r,t) = \hat{z} \frac{I}{N} \frac{1}{r} \delta(r - r_0 - \xi_i) \delta\left(\theta - \theta_i - \frac{\eta_i}{r_0}\right), \tag{3}$$

where δ is the Dirac delta function. The work done by this current filament on the deflecting mode is proportional to

$$W_i = \int dV \, \mathbf{A}_1 \cdot \mathbf{J}_i, \tag{4}$$

 0021-8979/93/74(9)/5877/3/$6.00

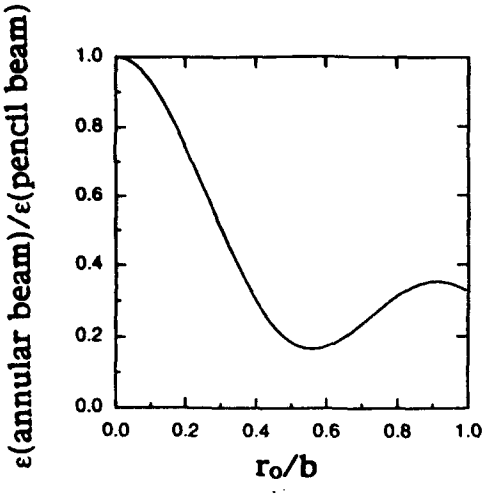

FIG. 1. Comparison of the BBU coupling constant ϵ between an annular beam of radius r_0 and an on-axis pencil beam ($r_0 \to 0$) with the same total current.

where the volume integral is performed over the cavity. In evaluating W_i, we should retain only the rf component of $\mathbf{J}_i$ in Eq. (3), since only the rf current performs work on the breakup mode. Upon substituting Eqs. (1)–(3) into Eq. (4), and summing over all i, we find the total work done

$$W=\sum_{i=1}^{N} W_i=-\frac{LIe}{m_0}\frac{v_0}{c}q\frac{[E'(r_0)]^2+[E(r_0)/r_0]^2}{\gamma(\omega-kv_0)^2} \qquad (5)$$

apart from a multiplicative constant that is independent of the beam's equilibrium position r_0. This energy transfer leads to growth of the BBU mode, which is described by the BBU dispersion relation:[8]

$$(\omega^2-\omega_0^2)(\omega-kv_0)^2=-2\omega_0^4\epsilon=-2\omega_0^4\epsilon_0(\epsilon/\epsilon_0), \qquad (6)$$

where ϵ is the coupling constant and ω_0 is the breakup mode frequency. In writing the last form of Eq. (6), we normalize ϵ in terms of ϵ_0, the coupling constant for an on-axis, pencil beam ($r_0 \to 0$). For the TM_{110} mode, $E=J_1(pr)$ and $\epsilon_0=0.422(\beta/\gamma)(I/1\ \text{kA})$. It is clear from Eq. (5) that

$$\frac{\epsilon}{\epsilon_0}=2\left\{[J_1'(pr_0)]^2+\left[\frac{J_1(pr_0)}{pr_0}\right]^2\right\}, \qquad (7)$$

which compares the BBU strength between an annular beam and a pencil beam of the same current. Note that this ratio reduces to unity in the limit $r_0 \to 0$.

Equation (7) is plotted in Fig. 1 as a function of r_0/b. It is seen from this figure that ϵ/ϵ_0 may be as small as 0.17 when the annular beam is located at $r_0=0.56b$. Note also that this location coincides with the minimum of the rf magnetic field of the deflecting mode. What this means is that an annular beam placed at this location can carry as much as $1/0.17=6$ times the current as an on-axis pencil beam, and suffer the same BBU growth. Another point worth noting is that BBU growth retains significant strength even if the annular beam is very close to the wall of the drift tube (cf. $r_0 \to b$ in Fig. 1). This result is unexpected since $E_l \to 0$ near a metallic wall. As a result, $\mathbf{J}_l \cdot \mathbf{E}_l \to 0$ and, superficially, one could hardly expect any transfer of power from the beam to drive the breakup mode.[9] The finite BBU strength as $r_0 \to b$ is another strong indication that the deflecting magnetic field is far more important than the axial rf electric field in driving BBU.

The importance of the rf magnetic field can be tested in an experiment in which a pencil beam is focused by a solenoidal magnetic field and is made to pass through a sequence of pillbox cavities, in which the first cavity is primed with microwaves at the TM_{110} mode.[10] BBU growth is monitored at the last cavity, before the beam exit. The above theory then predicts the *unusual* feature that BBU growth should be *much less* if the pencil beam is placed *off-axis*, than if the pencil beam were on-axis.[11] The BBU growth should be minimum if this pencil beam is placed at a distance of about 0.56 of the pillbox radius, where the rf magnetic field is minimum.

We also repeated the calculations for the higher order radial modes: TM_{120}, TM_{130}, TM_{140}, and TM_{150}. Fixing $r_0/b=0.56$, the ratio ϵ/ϵ_0 equals 0.16, 0.012, 0.037, and 0.013 for these four higher order modes, respectively. Thus, the annular beam still suffers substantially lower BBU growth, in the higher order deflecting modes, than an on-axis pencil beam of the same current.

In conclusion, the rf magnetic field is found to be much more important than the rf electric field in contributing to BBU growth. A simple proof-of-principle experiment is proposed to test this new finding. Annular beams are far more stable than an on-axis pencil beam, as a result.

We thank Professor Ronald Gilgenbach for his support and for many useful discussions. This work was supported in part by an SDIO/IST contract managed by ONR.

[1] V. Serlin and M. Friedman, Appl. Phys. Lett. 62, 2772 (1993); Y. Y. Lau, M. Friedman, J. Krall, and V. Serlin, IEEE Trans. PS-18, 553 (1990) and references therein; M. Friedman, Y. Y. Lau, J. Krall, and V. Serlin, U. S. Patent 5,132,638 (issued July 21, 1992); J. Krall, M. Friedman, Y. Y. Lau, and V. Serlin, IEEE Trans. EMC-34, 22 (1992).
[2] C. Chen, P. Catraras, and G. Bekefi, Appl. Phys. Lett. 62, 1579 (1993); See also, "Intense Microwave and Particle Beams III," Proc. Soc. Photo Opt. Instrum. Eng. SPIE 1629 (1992).
[3] G. Voss and T. Weiland, "The wakefield acceleration mechanism," Deutsches Electron-Synchrotron Internal Report DESY #M82-10 (1982); M82-079 (1982), Hamburg, Germany.
[4] M. Friedman, J. Krall, Y. Y. Lau, and V. Serlin, Phys. Rev. Lett. 63, 2468 (1989).
[5] W. K. H. Panofsky and M. Bander, Rev. Sci. Instrum. 39, 206 (1968); R. H. Helm and G. A. Loew, in *Linear Accelerators*, edited by R. P. Lapostolle and A. L. Septier (North-Holland, Amsterdam, 1970), p. 173.
[6] V. K. Neil, L. S. Hall, and R. K. Cooper, Part. Accel. 1, 111 (1970); 9, 213 (1979).
[7] A. W. Chao, B. Richter, and C. Y. Yao, Nucl. Instrum. Methods 178, 1 (1980); K. A. Thompson and R. D. Ruth, Phys. Rev. D 41, 964 (1990); R. L. Gluckstern, F. Neri, and R. K. Cooper, Part. Accel. 23, 37 (1988); C. L. Bohn and J. R. Delayen, Phys. Rev. A 45, 5964 (1992); D. Chernin and A. Mondeli, Part. Accel. 24, 685 (1985); G. Decker and J. M. Wang, Phys. Rev. D 38, 980 (1988); W. E. Martin, G. J. Caporaso, W. M. Fawley, D. Prosnitz, and A. G. Cole, Phys. Rev. Lett. 54, 685 (1985); D. Colombant, Y. Y. Lau, and D. Chernin, Part. Accel. 35, 193 (1991).
[8] Y. Y. Lau, Phys. Rev. Lett. 63, 1141 (1989).

[9] The rate of power transfer is proportional to the gradient of E_z, rather than E_z itself. This may be seen when one substitutes Eq. (3) into Eq. (4) and performs integration by parts.

[10] P. R. Menge, R. M. Gilgenbach, and Y. Y. Lau, Phys. Rev. Lett. 69, 2372 (1992); P. R. Menge, R. M. Gilgenbach, and R. Bosch, Appl. Phys. Lett. 61, 642 (1992).

[11] BBU growth on a pencil beam that is placed off-center can be easily calculated by using Eq. (4) instead of Eq. (5). We pretend that the total beam current is carried by the kth filament that enters Eq. (4). Although the BBU growth of such an off-center beam depends on θ_k, its coupling constant ϵ is still much less than ϵ_0, the value for an on-axis beam.